Fibroblast p38-MAPK signaling modulates cardiac function and phenotype in mouse models of inherited dilated and hypertrophic cardiomyopathy

Kristin Zabrecky

A thesis

submitted in partial fulfillment of the

requirements for the degree of

Master of Science

University of Washington

2021

Committee:

Jennifer Davis

Piper Treuting

Charles Frevert

Program Authorized to Offer Degree:

Department of Compartive Medicine

©Copyright 2021

Kristin Zabrecky

University of Washington

Abstract

Fibroblast p38-MAPK signaling modulates cardiac function and phenotype in mouse models of inherited dilated and hypertrophic cardiomyopathy

Kristin Zabrecky

Chair of Supervisory Committee:

Jennifer Davis

Departments of Bioengineering and Laboratory Medicine and Pathology

Inherited cardiomyopathies are common causes of heart failure in the general population that present with two main clinical phenotypes: dilated cardiomyopathy (DCM) and hypertrophic cardiomyopathy (HCM). Little is known regarding the pathogenesis and subsequent clinical impact of early extracellular matrix (ECM) remodeling in these diseases. By genetically modulating the ECM via fibroblast p38-MAPK, the mechanical basis of ECM-cardiomyocyte feedback and consequence on whole heart remodeling in DCM and HCM was examined via non-invasive and invasive physiology metrics. Both structural and functional phenotype was demonstrated to be susceptible to matrix modifications at the whole heart and cardiomyocyte level. This study demonstrates that fibroblast state and downstream matrix remodeling play an active role in the pathogenesis of cardiomyopathies and offers insights into early diagnostic tools and targeted therapeutic approaches.

Table of Contents

Acknowledgments

I would like to thank Darren Bugg and Amy Martinson for their care and maintenance of the animals in this study without whom none of this research would have been possible.

Thank you to Dr. Kristi Kooiker for her contribution of the demembranated multicellular and intact muscle measurements in this study.

Thank you to Logan Bailey and Bella Reichardt for their assistance with isolated myocyte metrics.

Thank you to the rest of the wonderful research team in the Davis Lab:
Ross Bretherton, Jagadambika Gunaje, Abby Nagle, Emily Olszewski, and Kalen Robeson.

And finally, I would like to thank my research mentor, Dr Jennifer Davis, her support and guidance throughout this project.

Dedication

This work is dedicated to the countless friends and family that have supported me throughout the years and to my aunt, Dr. Elizabeth Panke, who is living proof that you can do whatever you set your mind to and that the pursuit of research has the ability to change lives.

Introduction

Inherited cardiomyopathies are common causes of heart failure in the general population that present with two main clinical phenotypes: dilated cardiomyopathy (DCM) and hypertrophic cardiomyopathy (HCM). Both DCM and HCM are common, with conservative prevalence estimates around 1:250-500 and 1:500, respectively (McNally et al 2017, Mckenna et al 2020). DCM is characterized by ventricular chamber enlargement, systolic dysfunction, and eccentric hypertrophy, while HCM is characterized by reduced ventricular chamber dimensions, ventricular wall thickening, diastolic dysfunction, and increased risk of cardiac arrythmias (McKenna et al 2020). Both forms of cardiomyopathies are often linked to mutations that modulate the function and force generation of the sarcomere, the smallest contractile unit of the cardiomyocyte (Mckenna et al 2020, McNally et al 2013). These mutations are hypothesized to alter cardiac tension index, a predictive algorithm for cardiac remodeling defined as the time-tension integral of twitch force generated by a cardiomyocyte, and their altered contractility has prompted the development of therapeutics to directly modulate contractility itself (Davis et al 2016, Green et al 2016, NCT04572893)

What is important to also consider, however, is the contribution of factors outside the cardiomyocyte on cardiac structural and functional phenotype since cardiomyopathies have incomplete penetrance in that the identification of a known sarcomeric mutation does not necessarily correlate with expected clinical disease presentation even within members of the same family (Maron et al 2019, Greenberg et al 2021, Garfinkel et al 2018). It has therefore been suggested that multiple factors likely contribute to overall disease progression (Maron et al 2019). This is highlighted by a study examining a small molecule targeting sarcomere

contractility that was able to prevent progression of HCM in a small animal model but didn't reverse other pathologic features of disease, such as fibrosis (Green et al 2016). The excess accumulation of collagenous extracellular matrix (ECM), known pathologically as fibrosis, is an excellent predictor of adverse outcomes for patients with both HCM and DCM (Eijgenraam et al 2020, Gulati et al. 2013, Ho et al. 2010). While cardiac fibrosis is a hallmark of the pathophysiological progression of cardiomyopathies, our understanding of fibrosis is primarily derived from models of acute cardiac injury, such as myocardial infarction (MI) (Eijgenraam et al 2020). Therefore, little is known about what triggers fibrosis in a chronic disease such as a cardiomyopathy. For both DCM and HCM, interstitial and replacement fibrosis are present within myocardium and are often not observed until late in the disease course due to the insensitivity of current diagnostic tools such as late gadolinium enhancement MRI and invasive cardiac biopsies (Eijenraam et al 2020, Karaahmet et al 2010, Liu et al 2017). Gene expression profiling in cardiomyopathies, however, has demonstrated increases in pro-fibrotic genes well before the onset of classic clinical disease (Kim et al 2007, Ho et al 2010, Fujiu et al 2014, Liu et al 2019). One study by Junttila et al in 2018 even suggests that the presence and accumulation of fibrosis in absence of classical clinical presentation could be an early manifestation of the disease or even an alternative phenotypic expression of inherited cardiomyopathies all together. Additionally, a recent study by our lab demonstrated increased collagen fiber alignment and fibroblast proliferation that proceeded maladaptive ventricular remodeling in a DCM mouse model (unpublished data). Indeed, it is known that the arrangement, stiffness, and quantity of ECM, all of which are modified by fibrosis, can have structural, mechanical, functional consequences on the heart (Fomovsky et al 2010, Ward et al 2020). Thus, the pro-fibrotic pathways and early modification in ECM composition and mechanical properties likely to play a

significant role in overall clinical disease development and presentation. Therefore, selectively targeting the ECM could further elucidate the mechanical basis of ECM-cardiomyocyte feedback in cardiomyopathies.

Cardiac ECM is deposited and remodeled by a cell type known as the resident cardiac fibroblast, which can be targeted genetically in mice expressing an inducible Cre recombinase at the *Tcf21* locus (Czubryt 2019). Matrix deposition and remodeling are controlled by the cardiac fibroblast in response to a variety biochemical and mechanical cues which activate a diverse array of downstream signaling effectors leading to ECM protein synthesis and secretion (Davis et al 2014). A key component of this activation pathway is p38 mitogen-activated protein kinase (p38-MAPK) (Bretherton et al 2020). In *Tcf21*-targeted genetic mouse models, deletion of the *Mapk14* gene encoding for p38 inhibited fibroblast activation and the fibrotic response to cardiac injury, neurohumoral stimulation, and wound healing (Molkentin et al 2017). This inhibition of fibroblast p38 also highlighted its role in maintaining structural integrity of the heart since deletion led to cardiac rupture post MI (Molkentin et al 2017). In contrast, constitutively activating p38 through an upstream kinase, MKK6, induced fibroblast activation and accumulation of interstitial and perivascular fibrosis (Molkentin et al 2017). Therefore, it is clear that p38-MAPK significantly impacts the activation and function of fibroblast regulation on the ECM.

Fibroblasts can sense and respond to changes in muscle mechanics, but little understood in how the fibroblast responds to the altered mechanics of inherited cardiomyopathies and their function in disease pathogenesis (Herum et al 2017). By modulating the ECM through genetic

manipulation of p38-MAPK in the cardiac fibroblast, the role of fibroblast activation and subsequent of matrix remodeling on disease progression can be investigated in DCM and HCM. It is known that cardiomyocytes can also sense and respond to this mechanical environment through mechanotransduction pathways that modulate cardiomyocyte function and contractility (Munch et al 2021, Sewanan et al 2019). Therefore, the effect on cardiomyocyte function from extracellular influences could in turn compound or even counteract the altered function and force generation from DCM and HCM sarcomeric mutations that determine clinical disease presentation. Thus, it is hypothesized that modulating matrix remodeling through fibroblast p38-MAPK causes reciprocal changes to cardiomyocyte contractility which will manifest as changes to whole heart structural and functional phenotype.

Since increasing cardiac stiffness has been shown to elicit structural remodeling and reduce contractile function in cardiomyocytes (Munch et al 2021, Galie et al 2013), it is hypothesized that increasing ECM deposition through fibroblast p38 activation would further promote the hypo-contractile function of DCM cardiomyocytes leading to exacerbated dilated remodeling and systolic dysfunction at the whole heart level. In contrast, activation of p38 would dampen the hyper-contractile function of HCM cardiomyocytes leading to reduced concentric hypertrophy, systolic function, and diastolic dysfunction. Additionally, it is hypothesized that the reduced ECM deposition by knockout of fibroblast p38 would in turn improve contractility in DCM cardiomyocytes leading to reduced maladaptive dilated remodeling and improved systolic function while further promoting the hyper-contractile HCM cardiomyocytes leading to exacerbated concentric remodeling, hyper-dynamic systolic function, and diastolic dysfunction.

To investigate these questions, two characterized and diametrically opposed mouse models of DCM and HCM were utilized (Davis et al 2016). These models have transgenic manipulation of the sarcomere calcium binding thin filament protein, cardiac troponin C (cTnC), by functionally opposed I61Q and L48Q mutations leading to quantitative shifts in calcium binding and reduced and enhanced tension production respectively (Davis et al 2016, Wang et al 2013, Wang et al 2012). While mutations of cTnC are rare in human inherited DCM and HCM, rationally introducing mutations into this protein allows for the direct control of the sarcomeric calcium-tension relationship while also recapitulating key whole heart phenotypic characteristics of DCM and HCM (Davis et al 2016, Kalyva et al 2014, Reinoso et al 2020). The DCM phenotype in I61Q mice is characterized by systolic dysfunction and a dilated and hypertrophied structural phenotype with increased left ventricular diameter, reduced left ventricular wall thickness, and increased heart to body weight ratio, a measure of cardiac hypertrophy (Davies et al 2016). In contrast, while initially masked by the high adrenergic drive and heart rate of the mouse, the HCM phenotype of L48Q mice can be unmasked by both drug and surgical intervention to demonstrate increased heart weight to body weight ratio, increased left ventricular wall thickness, reduced left ventricular diameter, hyper-dynamic systolic function, and diastolic dysfunction (Davies et al 2016). By genetically manipulating matrix remodeling through fibroblast p38-MAPK in these mouse models, the consequences on whole heart cardiomyopathy phenotype were examined via both non-invasive and invasive metrics.

Materials and Methods

Animal Models and Procedures

All experimentation on animals was approved by the Institutional Animal Care and Use Committee at University of Washington.

WT, I61Q, and L48Q cTnC transgenic mouse variants with an alpha myocin heavy chain (αMHC) promotor were previously described in Davis et al 2016. This bigenic system requires the presence of the tetracycline transactivator (tTa) for cTnC transgene expression. Doxycycline chow (625mg/kg) can be provided to suppress cTnC transgene expression and can be removed to allow transgene expression when desired; however, doxycycline was not provided at any time to allow for cTnC transgene activation throughout the experiments. Transgene expression has been shown to not have lethal consequences during or after development (Davis et al. 2016).

Lox-P targeted *Mapk14* mice with a tamoxifen inducible MerCreMer on the *Tcf21* genomic loci were previously described in Molkentin et al. 2017 and used to knockout p38 in resident cardiac fibroblasts (referred to as P38). Mice containing the tamoxifen inducible constitutively active MKK6 transgene on the *Tcf21* genomic loci were previously described in Molkentin et al. 2017 and used to activate downstream p38 in resident cardiac fibroblasts (referred to as MKK6).

cTnC transgenic mice with either I61Q or L48Q were crossed to either P38 or MKK6 mice to manipulate the fibroblast p38-MAPK pathway. Tamoxifen induction was initiated at 1 month of age by once daily intraperitoneal injections in peanut oil (40mg/kg) for 5 days then maintained

on tamoxifen chow (40-48mg/kg/day). Mice were collected for terminal cardiac harvest at 4 months of age unless otherwise specified.

Control mice were defined as either non-transgenic (NTG), tTA, p38F/F, or TCF21+/-. These genotypes have been previously demonstrated to be phenotypically equivalent to appropriate inbred controls and were confirmed to be equivalent in this study via echocardiography at 4 months of age (Supp table 1) (Davis et al 2016, Molkentin et al 2017).

For echocardiography measurements, mice at 4 months of age were anesthetized via inhalation of isoflurane anesthesia (induction 5%, maintenance 1.5%), hair removed via Nair (Church & Dwight Co. Inc. Ewing, NJ), and measured with the Vevo2100 or Vevo3100 Imaging System (Fuji Film Visual Sonics, Inc. Toronto, ON) using a 15-MHz transducer. M-mode measurements were taken of the parasternal short axis view for ejection fraction, ventricular chamber dimensions, and wall thicknesses during systole and diastole.

In vivo hemodynamics were measured in isoflurane anesthetized mice (induction 5%, maintenance 1.5%) using high fidelity pressure-volume catheters (1.2F, Transonic System Inc) inserted into the left ventricle through the right carotid artery. Heart rate was restricted to 420-500bpm, and temperature was maintained at 37°C. Volume calibration was performed via cuvette calibration.

Transverse aortic constriction (TAC) was used to generate pressure overload on the heart and compensatory hypertrophy. This procedure has been previously described (Kaiser et al., 2004).

In these experiments, a 6-0 silk ligature was permanently tied around the aorta and a 26-27 gauge bent needle between the right brachiocephalic and left common carotid arteries to induce a defined constriction in blood flow. Hearts were examined after 2 weeks of TAC via echocardiography and terminal heart collection. Sham surgery consisted of a median sternotomy.

Demembranated Multicellular Measurements

Experiments were performed as described in Moussavi-Harami et al 2015. Excised hearts were demembranated overnight at 4 ºC in 50:50 (vol:vol) glycerol:relaxing solution (in mM: 100 KCl, 10 imidazole, 2 EGTA, 5 $MgCl_2$, and 4 ATP) containing 1X protease inhibitor cocktail (Sigma-Aldrich P8340) and 1% triton X-100. Hearts were transferred to fresh glycerol:relaxing solution without triton X-100, then stored at -20 ºC for up to one week. Right ventricular multicellular preparations were dissected, secured between aluminum t-clips, and then mounted between a motor (Aurora Scientific, Model 312B) and force transducer (Aurora Scientific, Model 403A). Preparations were moved to a bath containing experimental relaxing solution (pCa 9.0) at pH 7.0 and 15 °C containing (in mM): 15 phosphocreatine, 15 EGTA, 80 MOPS, 1 free Mg^{2+}, 10^{-9} Ca^{2+}, 1 DTT, and 5 Mg_2ATP at 15 ºC. For Ca^{2+} sensitivity curves, the experimental relaxing solution was made with varying levels of free calcium from pCa^{2+} 4.0 to 6.2 ($pCa^{2+} = -\log[Ca^{2+}]$). Preparations were lengthened to sarcomere length of ~2.3 µm then moved between solution baths where force was measured. Analysis was performed using custom LabView software.

Histology

Hearts were fixed in 37% neutral buffered formalin and processed and embedded in paraffin wax. 5 micron short axis cross sections at the level of the left ventricular papillary muscles were

stained with pico sirus red and imaged at 2x and 10x on an Olympus BX41 microscope. Percent fibrosis was calculated via Image J software to determine the percent collagen (red) to total heart tissue (green).

Myocyte Isolation and Measurements

Mice were injected with heparin (100U) via intraperitoneal injection. After 10 minutes, mice were euthanized with Beuthanasia-D (phenytoin 2.5mg, pentobarbital 19.5mg) via intraperitoneal injection. Hearts were removed and the aorta cannulated. Hearts were perfused in a perfusion solution (NaCl 135mM, KCl 4.6mM, KH_2PO_4 0.6mM, $Na_2HPO_4xH_2O$ 0.6mM, $MgSO_4x7H_20$ 1.2mM, HEPES free acid 20mM, taurine 30mM, glucose 5mM, and BDM) for 5 minutes then digested with perfusion solution with liberase TH and 10mM Ca^{2+}. Isolated ventricular myocytes were filtered through a 200um filter and allowed to settle by gravity. Myocyte pellets were washed with perfusion solution with increasing calcium concentrations (0.125mM, 0.25mM, 0.5mM) and settled by gravity between each wash. Myocyte pellets were resuspended in Normal Tyrode's (NT) solution (NaCl 137mM, KCl 5.4mM, MgCl2 0.5mM, CaCl2xH20 1.2mM, HEPES 10mM, glucose 5mM) and plated on cover slips for mechanical properties.

Myocyte mechanical properties for sarcomere length, maximum velocities, and time to peak and baseline were recorded using an IonOptix contractility system (Milton, MA) (1Hz, 37°C, 1.2 mM Ca^{2+}). A separate subset of myocytes were incubated with 2uM fura-2 acetoxy-methyl ester for 30 minutes. The Ca^{2+} transient ratio, amplitude, and time to transient ratio recovery or return

to baseline were recorded using the IonOptix system at 10V pacing. The all data was analyzed via the IonWizard data analysis software.

Intact Muscle Measurements

Experiments were done as previously described by Powers et al 2020. Unbranched trabecula or papillary muscle was dissected from the right ventricle of mouse hearts that were excised then perfused with oxygenated (95% O_2/ 5% CO_2) modified Krebs buffer containing (in mM) 118.5 NaCl, 5 KCl, 1.2 $MgSO_4$, 2 NaH_2PO_4, 25 $NaHCO_3$, 0.1 $CaCl_2$, and 10 glucose, with 20 mM 2,3-butanedione 2-monoxime added to minimize contraction and subsequent damage during dissection. Trabecula were then transferred to a continuously perfused bath containing oxygenated modified Krebs buffer with high calcium (1.8 mM $CaCl_2$) at 30 ºC and mounted between a force transducer (Cambridge Technology, model 400A) and a length-controlling motor (Aurora Scientific, model 300C). Twitches were elicited by field stimulation at 1 Hz with oscillating polarity. Trabecular length was set to just above slack and allowed to pace for 20 minutes. Measurements were then taken at an optimal length just below where maximal twitch peak occurs. Twitches were analyzed using custom code with MATLAB software (version R2021a, MathWorks).

Statistics

Data was expressed as mean+/-SD unless otherwise stated. Unpaired t-tests were used to determine statistical significance in experiments with 2 groups. One way analysis of variance (ANOVA) was used to determine statistical significance in experiments with more than 2 groups using Tukey's multiple comparison test to determine significance between groups.

Results

Reduced calcium sensitivity of tension generation results in a DCM phenotype in a mixed strain mouse model

To investigate the effects of matrix remodeling on DCM cardiac structure and function, I61Q mice with the cTnC tetracycline bi-transgenic inducible system (Figure 1A) were crossed with established mouse models of fibroblast targeted manipulation of p38-MAPK (Davis et al 2016, Molkentin et al 2017). Knockout of p38 in resident cardiac fibroblasts was achieved via the tamoxifen inducible deletion of the *Map14* gene (mouse referred to as P38), while activation was achieved via the tamoxifen inducible constitutively activated MKK6 transgene, an upstream kinase of p38 (mouse referred to as MKK6) (Figure 1B-C). Tamoxifen administration was initiated at 1 month of age via once daily intraperitoneal injections for 5 days then maintained on tamoxifen chow until 4 months of age (Figure 1D).

Previously, the structural and functional DCM phenotype of the I61Q mouse was characterized on an inbred FVB/N mouse strain (Davis et al 2016). Utilizing an inbred strain is generally preferred to reduce trait variability and reliably study genome manipulations without additional genetic confounders (Tuttle et al 2018). However, to allow for the targeted manipulation of the fibroblast p38-MAPK *in-vivo*, the inbred FVB/N I61Q mouse was crossed with the C57BL/6 P38 and MKK6 mice. Due to the genetically undefined nature of mixed crosses and outbred stocks, genetic quality control is based on assessing expected phenotypic traits (Benavides et al 2019). Thus, it is hypothesized that the I61Q cTnC transgene function and DCM phenotype will be maintained on a mixed strain mouse model.

The I61Q cTnC transgene reduces calcium (Ca^{2+}) sensitivity of contraction by disrupting the cTnC Ca^{2+} binding site through intra-molecular interactions (Davis et al 2016, Wang et al 2013). To investigate if the expected 161Q cTnC transgene function was maintained in a mixed strain background, Ca^{2+} of tension generation was measured in demembranated cardiac muscle strips. The hyperbolic relationship between Ca^{2+} and muscle contraction for I61Q and controls was plotted on a normalized force-pCa^{2+} plot in which pCa^{2+} is defined as the $-\log_{10}$ of Ca^{2+} concentration. Compared to controls, I61Q had a rightward shift of this curve indicating reduced Ca^{2+} sensitivity of tension generation (Figure 1E). This was quantitively demonstrated with a reduced $pCa_{50,}$ which indicates the I61Q mutant required more Ca^{2+} than controls to reach 50% of maximum force generation (Figure 1F). Overall, these results confirm the expected reduced Ca^{2+} sensitivity of force generation of I61Q cTnC on a mixed strain background (Davis et al 2016, Wang et al. 2013).

To confirm the expected DCM structural and functional phenotype of I61Q with the mixed strain, I61Q and control mice were examined via echocardiography and terminal cardiac evaluation at 4 months of age without tamoxifen administration. I61Q mice demonstrated the characteristic cardiac remodeling of DCM with increased heart weight to body weight ratio, increased left ventricular diameter, and reduced left ventricular wall thickness (Figure 1G-I). I61Q mice additionally demonstrated systolic dysfunction as measured by reduced ejection fraction (Figure 1J). Overall, the structural and functional DCM phenotype in mixed strain I61Q mice mirrored what was previously illustrated in inbred mice (Davis et al. 2016).

Loss of fibroblast p38 rescues 161Q ventricular chamber dilation, systolic dysfunction, and impaired contractility

To investigate the hypothesis that reduced ECM deposition by knockout of fibroblast p38 would improve DCM dilated structural phenotype and systolic function, I61Q mice were crossed with P38 mice and started on tamoxifen at 1 month of age as described in Figure 1D (mice referred to as P38 I61Q). The effect of p38 knockout on I61Q cTnC transgene function was evaluated via Ca^{2+} sensitivity of tension generation in demembranated cardiac muscle strips. I61Q with p38 knockout had reduced Ca^{2+} sensitivity of tension generation with a rightward shift of the force-pCa^{2+} curve and reduced pCa_{50} comparable to what was observed in I61Q alone (Figure 2A-B). Thus, the loss of fibroblast p38 did not alter the Ca^{2+} sensitivity of tension generation of the I61Q mutant.

To explore the structural and functional consequences of loss of fibroblast p38 on I61Q phenotype, control, P38, I61Q, and P38 I61Q, mice were examined via echocardiography and terminal cardiac evaluation at 4 months of age. In contrast to inbred and mixed strain I61Q mice not given tamoxifen, there was no change in heart weight to body weight ratio in I61Q compared to controls (Figure 2C). However, the dilative DCM phenotype of I61Q was demonstrated in a trend of increased left ventricular diameter and reduced left ventricular wall thickness that were both rescued with p38 knockout (Figure 2D-E). Additionally, I61Q mice exhibited DCM systolic dysfunction with reduced ejection fraction that was also rescued with p38 knockout (Figure 2F).

The use of invasive hemodynamic measurements allows for a comprehensive and direct assessment of cardiac structure, function, and muscle parameters and is considered the gold

standard to assess ventricular performance (Liu et al 2019). This then allows for a more in-depth evaluation of the functional role of mutations on cardiac muscle physiology (Cingolani et al 2011, Townsend 2016). To investigate not only the I61Q DCM phenotype further but also the loss of p38 on DCM phenotype, control, P38, I61Q, and P38 I61Q mice were subjected simultaneous measurement of left ventricular pressure and volume by pressure-volume (PV) loop analysis. The expected dilative DCM structural phenotype of I61Q was not demonstrated via PV-loop end diastolic volume (Figure 2G). Stroke work, a measure of systolic function, however, did demonstrate the previously observed I61Q systolic dysfunction that was again rescued by p38 knockout. (Figure 2H). One of the primary advantages of PV loop analysis is the capability to evaluate load-independent parameters of contractility, the intrinsic ability of cardiac muscle to generate force (Cingolani et al 2011). These parameters are evaluated by reducing venous return through transient caudal vena cava occlusion. The end systolic pressure volume relationship (ESPVR) is the maximal pressure of the ventricle at a given volume and thus a measure of muscle contractility (Cingolani et al 2011). By this metric, I61Q exhibited impaired muscle contractility that was improved with p38 knockout (Figure 2I). While systolic dysfunction and impaired contractility are considered primary pathologies in DCM, diastolic dysfunction is also important in disease pathogenesis (Kashyap et al 2014). Diastolic function was assessed by tau, or the isovolumetric relaxation constant, that represents the exponential decay of ventricular pressure during isovolumic relaxation (Chowdhury et al 2015). Tau was prolonged in I61Q indicating diastolic dysfunction that was unchanged by p38 knockout (Figure 2J). Additionally, the passive stiffness of the ventricle in diastole was assessed via the load-independent metric EDPVR or end diastolic pressure volume relationship (Liu et al 2019). This value, however, did not indicate restrictive passive stiffness in any group (Figure 2K). Overall,

the utilization of invasive hemodynamics further demonstrated the rescue of DCM systolic function and contractility with p38 knockout as observed via echocardiography while unaffecting DCM diastolic dysfunction. A comprehensive table of the PV loop values illustrated in Figure 2 as well as additional volume, pressure, and load independent measurements are listed in Suppl Table 2.

Since the knockout of p38 was previously demonstrated to inhibit the fibrotic response in resident cardiac fibroblasts, fibrosis was quantified in hearts stained with pico-sirus red by calculating the amount of collagen (red) to relative to total heart area (green) in cross-sections at the level of the papillary muscles (Figure 2L-M) (Molkentin et al 2017). While not significant, I61Q hearts did have a trend of increased fibrosis (Figure 2L); however, the overall total percentage was low for all groups suggesting additional ECM parameters, such as alignment, fibroblast proliferation, and stiffness, should also be explored to investigate the specific mechanisms of reduced matrix remodeling on improved DCM phenotype.

Loss of fibroblast p38 improves I61Q cardiomyocyte mechanics by altered Ca^{2+} handling

Since the knockout of p38 in fibroblasts improved the I61Q DCM phenotype, the cardiomyocyte was evaluated to test the hypothesis that this shift in whole heart phenotype was due to the effects of matrix remodeling on individual cardiomyocyte function and contractility. The cardiomyocyte has many ways to alter contractility such as through sarcomere number and arrangement, Ca^{2+} handling, microtubule remodeling, response to soluble mediators, and others (Dornll et al 2004, Ward et al 2020). To quantify two of these metrics, sarcomere length and intracellular Ca^{2+} were measured in isolated cardiomyocytes using the Myocyte Calcium and

Contractility System (IonOptix). I61Q myocytes had reduced sarcomere shortening, an indicator of impaired contractility, as well as reduced contraction time and reduced maximal rate of change during contraction (Figure 3A-C) This reduction in contractility was not accompanied by a change in intracellular Ca^{2+} kinetics (Figure 3E-H). I61Q myocytes with p38 knockout, however, had improved sarcomere shortening, contraction time, and maximal rate of change during contraction compared to I61Q (Figure 3A-C). These improvements in contractility were accompanied by increases in Ca^{2+} transient amplitude, time of Ca^{2+} release, and rate of Ca^{2+} release as well as reduced Ca^{2+} decay time compared both I61Q and controls (Figure 3 E-H). These results suggest that modulation of intracellular Ca^{2+} kinetics by manipulating matrix remodeling could play a direct role in improving contractility and function in DCM cardiomyocytes.

Fibroblast p38 activation increases fibrosis but does not alter I61Q DCM ventricular chamber dilation or systolic dysfunction

To investigate the hypothesis that increased ECM deposition by activation of fibroblast p38 would exacerbate DCM dilated structural phenotype and systolic dysfunction, I61Q mice were crossed with MKK6 mice and started on tamoxifen at 1 month of age as described in Figure 1D (mice referred to as MKK6 I61Q). The effect of p38 activation on I61Q cTnC transgene function was evaluated via Ca^{2+} sensitivity of tension generation in demembranated cardiac muscle strips. I61Q with p38 activation had reduced Ca^{2+} sensitivity of tension generation with a rightward shift of the force-pCa^{2+} curve and reduced pCa_{50} comparable to what was observed with I61Q alone (Figure 4A-B). Thus, the activation of fibroblast p38 did not alter the Ca^{2+} sensitivity of force generation in the I61Q mutant.

To explore the structural and functional consequences of activated fibroblast p38 on I61Q phenotype, control, MKK6, I61Q, and MKK6 I61Q mice were examined via echocardiography and terminal cardiac evaluation at 4 months of age. Again, there was no change in heart weight to body weight ratio of I61Q compared to controls (Figure 4C); however, as previously observed, I61Q mice exhibited a dilated DCM phenotype with increased left ventricular diameter and trend of reduced left ventricular wall thickness (Figure 4D-E). I61Q mice also demonstrated DCM systolic dysfunction via reduced ejection fraction (Figure 4F). The activation of p38, however, did not alter these parameters of DCM structural or functional phenotype (Figure 4D-F)

PV loop analysis was utilized to continue to explore the DCM phenotype with p38 activation. While there was no change in parameters measuring ventricular volume, contractility, and passive stiffness, I61Q systolic dysfunction with and without p38 activation was confirmed via reductions in stroke work (Figure 4G-I,K). Additionally, the I61Q diastolic function was further impaired with p38 activation via increased isovolumetric relaxation constant tau (Figure 4J). Overall, the utilization of invasive hemodynamics confirmed the echocardiography findings of unaltered DCM systolic dysfunction while also demonstrating further diastolic dysfunction with p38 activation. A comprehensive table of the PV loop values illustrated in Figure 4 as well as additional volume, pressure, and load independent measurements are listed in Suppl Table 3.

Since activation of p38 in resident cardiac fibroblasts has been demonstrated to increase cardiac fibrosis, fibrosis was quantified in hearts stained with pico-sirus red by calculating the amount of collagen (red) to relative to total heart area (green) in cross-sections at the level of the papillary

muscles (Molkentin et al 2017). I61Q with p38 activation had quantitively increased fibrosis that was visually apparent throughout the myocardium. (Figure 4L-M). This increase could account for the p38 activation associated I61Q diastolic impairment since diastolic dysfunction has been associated with increased fibrosis and profibrotic cytokines, however, more work is needed to further investigate the impact of fibrosis as well as additional ECM metrics on diastolic function to elucidate specific mechanisms in this mouse model (Tanaka et al 2011).

Enhanced calcium sensitivity of tension generation suggests a HCM phenotype in a mixed strain mouse model

To investigate the effects of matrix remodeling on HCM cardiac structure and function, L48Q mice with the cTnC tetracycline bi-transgenic inducible system (Figure 5A) were crossed with the tamoxifen inducible P38 and MKK6 mice (Figure 5B-C). Tamoxifen administration was initiated at 1 month of age via once daily intraperitoneal injections for 5 days then maintained on tamoxifen chow until 4 months of age (Figure 5D). Again, to allow for this *in-vivo* targeted manipulation of the fibroblast p38-MAPK pathway, the inbred FVB/N L48Q mouse was crossed with the C57BL/6 P38 and MKK6 mice. Thus, similarly to I61Q, it is hypothesized that the L48Q cTnC transgene function and HCM phenotype will be maintained on a mixed cross mouse background.

The L48Q cTnC transgene enhances calcium (Ca^{2+}) sensitivity of contraction through destabilizing the closed cTnC structure and enhancing Ca^{2+} binding (Davis et al 2016, Wang et al 2012). To investigate if the expected L48Q cTnC transgene function is maintained on a mixed strain background, Ca^{2+} sensitivity of tension generation was measured in demembranated

cardiac muscle strips. Compared to controls, L48Q had a leftward shift of the force-pCa^{2+} curve indicating enhanced Ca^{2+} sensitivity of tension generation (Figure 5E). This was quantitively demonstrated with an increased $pCa_{50,}$ which indicates the L48Q mutant required less Ca^{2+} than controls to reach 50% of maximum force generation (Figure 5F). Overall, these results confirm the expected enhanced Ca^{2+} sensitivity of tension generation of L48Q cTnC on a mixed strain background (Davis et al 2016, Wang et al. 2012).

Second, to confirm the expected HCM structural and functional phenotype of L48Q on the mixed strain, L48Q and control mice were subjected to 2 weeks of transaortic constriction (TAC) to induce pressure overload and compensatory cardiac hypertrophy to unmask the HCM phenotype (Davis et al 2016). While not significant, L48Q mice after TAC had a trend of concentric hypertrophy via reduced left ventricular diameter and increased left ventricular wall thickness and enhanced systolic function via increased ejection fraction compared to controls (Figure 5H-J). The heart weight to body weight ratio, however, was variable and not altered from controls (Figure 5G). These results are preliminary and only suggest the L48Q phenotype is present on the mixed strain background, so more work is needed to truly confirm the expected HCM phenotype.

Loss of fibroblast p38 enhances L48Q stroke work but does not alter reduced ventricular diameter or enhanced ejection fraction

To investigate the hypothesis that reduced ECM deposition by knockout of fibroblast p38 would exacerbate HCM concentric structural phenotype, hyper-dynamic systolic function, and diastolic

dysfunction, L48Q mice were crossed with P38 mice and started on tamoxifen at 1 month of age as described in Figure 5D (mouse referred to as P38 L48Q).

To explore the structural and functional consequences of loss of fibroblast p38 on L48Q phenotype, control, P38, L48Q, and P38 L48Q mice were examined via echocardiography and terminal cardiac evaluation at 4 months of age. While there was no difference in heart weight to body weight ratio or left ventricular wall thickness, the concentric HCM phenotype of L48Q was suggested via reduced left ventricular diameter (Figure 6A-C) Additionally, L48Q demonstrated HCM hyper-dynamic systolic function via increased ejection fraction (Figure 6D). The knockout of p38, however, did not alter these parameters of HCM structural and functional phenotype (Figure 6B,D)

PV loop analysis was utilized to continue to explore the HCM phenotype with p38 knockout. While there was no change for parameters measuring ventricular volume and contractility between all groups, stroke work was increased in L48Q with p38 knockout compared to L48Q alone suggesting further hyper-dynamic systolic function (Figure 6E-G). This finding is in contrast to the similar ejection fraction observed between L48Q with and without p38 knockout via echocardiography (Figure 6D). It can be argued ejection fraction, while being the most widely used metric for systolic function due its non-invasive measurement technique, is not as specific for systolic function since it is sensitive to load dependent values and changes in cardiac geometry (Borlaug et al 2009). Therefore, stroke work could be a better metric for systolic function in this model; however, more work is needed to validate this finding due to the lack of significant change in additional metrics of systolic function and contractility via PV loops (Supp

table 4). The lack of classic HCM pathology of diastolic dysfunction and impaired filling was surprising in L48Q mice (Figure 6-I, Supp table 4) (McNally et al 2013). Utilizing either a TAC model or beta-blockers to unmask the full HCM phenotype is needed to truly investigate the role of matrix remodeling in this mouse model. A comprehensive table of the PV loop values illustrated in Figure 6 as well as additional volume, pressure, and load independent measurements are listed in Suppl Table 4.

Since the knockout of p38 was previously demonstrated to inhibit the fibrotic response in resident cardiac fibroblasts, fibrosis was quantified in hearts stained with pico-sirus red by calculating the amount of collagen (red) to relative to total heart area (green) in cross-sections at the level of the papillary muscles (Figure 6J-K) (Molkentin et al 2017). The lack of significance and low overall total percentages promote further investigation into additional ECM metrics, such as alignment, fibroblast proliferation, and stiffness, in L48Q models both with and without unmasking the HCM phenotype to fully investigate specific mechanisms on whole heart phenotype this mouse model (Figure 6I).

Fibroblast p38 activation promotes diastolic dysfunction while rescuing HCM cardiac diameter and hyper-dynamic systolic function

To investigate the hypothesis that enhanced ECM deposition by activation of fibroblast p38 would reduce HCM concentric structural phenotype, hyper-dynamic systolic function, and diastolic dysfunction, L48Q mice were crossed with MKK6 mice and started on tamoxifen at 1 month of age as described in Figure 5D. (Mouse referred to as MKK6 L48Q).

To explore the structural and functional consequences of activation of fibroblast p38 on L48Q phenotype, control, MKK6, L48Q, and MKK6 L48Q mice were examined via echocardiography and terminal cardiac evaluation at 4 months of age. While there was no difference in heart weight to body weight ratio or left ventricular wall thickness, the concentric HCM phenotype of L48Q was again suggested via reduced left ventricular diameter (Figure 7A-C) Additionally, L48Q demonstrated HCM hyper-dynamic systolic function via increased ejection fraction (Figure 7D). The activation of p38, however, rescued these parameters of HCM structural and functional phenotype (Figure 7B,D)

PV loop analysis was utilized to continue to explore the HCM phenotype with p38 activation. While there was no change for parameters measuring ventricular volume, systolic function, contractility, or passive stiffness between all groups, diastolic function via increased tau was impaired in L48Q with p38 activation (Figure 7E-I). This evidence of diastolic dysfunction with p38 activation was similarly observed in I61Q mice (Figure 4J), thus again providing evidence that p38 activation and subsequent matrix changes influences diastolic metrics. However, utilizing either a TAC model or beta-blockers to unmask the full HCM phenotype is needed to truly investigate the role of matrix remodeling of these as well as other phenotypic metrics in this mouse model. A comprehensive table of the PV loop values illustrated in Figure 6 as well as additional volume, pressure, and load independent measurements are listed in Suppl Table 5.

Since activation of p38 in resident cardiac fibroblasts has been demonstrated to increase cardiac fibrosis, fibrosis was quantified in hearts stained with pico-sirus red by calculating the amount of

collagen (red) to relative to total heart area (green) in cross-sections at the level of the papillary muscles (Molkentin et al 2017). While not significant and highly variable, the preliminary results suggest increased fibrosis with p38 activation (Figure 7J-K). This increase could account for the p38 activation associated L48Q diastolic impairment as well as rescue of HCM structure and function, however, more work is needed to confirm this finding, further characterize the L48Q HCM phenotype, and investigate additional ECM metrics to elucidate specific mechanisms in this mouse model

Manipulation of fibroblast p38-MAPK pathway alters I61Q predictive tension index

Since it has been demonstrated, especially with the loss of fibroblast p38 in I61Q mice, that altering matrix remodeling can have consequences on whole heart phenotype, it was hypothesized that the changes to cardiomyocyte contractility that led to these altered phenotypes can be used to predict the cardiac remodeling in these models. Davis et al in 2016 demonstrated that the cardiomyocyte force generation can be used to predict direction and magnitude of cardiac remodeling in DCM and HCM murine models, including I61Q and L48Q, and human mutants. This was done using the "tension index" or time-tension integral of twitch force generated by a cardiomyocyte to predict changes in ventricular chamber dimension, wall thickness, and cardiac mass. Thus, it is hypothesized that the impact on cardiac remodeling from modulating the matrix will be predicted using the tension index.

To investigate this question, the force over time in intact muscle strip twitches was measured. As observed previously, I61Q and L48Q mice had reduced and enhanced average force generation compared to controls respectively (Figure 8A) (Davis et al 2016). The average force generation

was slightly enhanced and reduced compared to controls by manipulating the fibroblast through knocking out and activation of p38 respectively (Figure 8B-C). When applied to I61Q, manipulating fibroblast p38 either through knockout or activation both improved I61Q force generation (Figure 8B-C)

The tension index was calculated via the normalized integral under the force-time curve (Figure 8D). These values were plotted to visually predict the magnitude and direction towards either dilative, indicated as negative values, or concentric, indicated as positive values, hypertrophy. As previously demonstrated, the tension index for both I61Q and L48Q correlated with the observed left ventricular dimensions via echocardiography with I61Q exhibiting a dilated phenotype and L48Q a concentric phenotype (Figure 2E-F, Figure 6B) (Davis et al 2016). When manipulating the fibroblast p38-MAPK pathway, the tension index shifted both slightly positive, for p38 knockout, and negative, for p38 activation (Figure 8E). By applying this to I61Q mice, both tension index values for knockout and activation of p38 were negative compared to controls but less negative compared to I61Q alone (Figure 8E). This predictive index correlated well with the observed improvement of left ventricular dimensions in I61Q with p38 knockout mice via echocardiography (Figure 2E-F); however, the tension index values for I61Q with p38 activation were highly variable, even within measurements from the same mouse, making interpretation of this index difficult and did not correlate with the dilated left ventricular diameter observed in these mice (Figure 4D). While L48Q with both p38 knockout and activation have yet to be evaluated using this predictive index, based on the tension indexes for knocking out and activating p38 as well as the evidence that ECM from HCM myocardium can affect myocyte force generation, it was hypothesized that tension index would be more and less positive,

respectivelym compared to L48Q and would correlate with resulting structural phenotype (Figure 8E) (Sewanan et al 2019).

Discussion

While the pathogenesis of inherited cardiomyopathies is complex, inherited cardiomyopathies are still broadly defined by their genetic associations, characteristic maladaptive remodeling, and resulting clinical manifestations. This study demonstrates that fibroblast state and downstream matrix remodeling play an active role in the pathogenesis of cardiomyopathies. By manipulating the p38-MAPK pathway in the cardiac fibroblast, it is demonstrated that the ECM provides a dynamic cue to the cardiomyocytes and can play an active role in determining not only cardiac structure but also cardiomyocyte and whole organ function. While it is well known that matrix changes are associated with inherited cardiomyopathies, they are traditionally characterized late in the disease process and the pathogenesis is not well understood (Eijgenraam et al 2020). Growing evidence that changes to the matrix can precede clinical disease opens an intriguing therapeutic target for the treatment of cardiomyopathies: the ECM (Kim et al 2007, Ho et al 2010, Fujiu et al 2014, Liu et al 2019). This study targets the matrix by way of the fibroblast p38-MAPK pathway early in the disease process to investigate the consequences on whole heart structure and function in the two diametrically opposed transgenic mouse models for DCM and HCM, I61Q and L48Q respectively, utilizing common cardiac physiologic metrics through echocardiography and invasive hemodynamics.

Overall, the functional effect of fibroblast p38 knockout in both DCM and HCM improved or further enhanced systolic function respectively while activation of p38 elicited diastolic dysfunction (Figures 2,4,6,7). Structurally, knockout of p38 in DCM and the activation of p38 in HCM improved ventricular chamber dimensions via echocardiography (Figure 2,7). There are several features of the ECM regulated by the fibroblast p38-MAPK pathway that could account

for these modifications of whole heart functional and structural phenotype (Camelliti et al 2005). Matrix remodeling involves changes to the quantity, composition, and alignment of the ECM that directly alter the mechanical environment surrounding the cardiomyocyte (Lopez et al 2015, Bretherton et al 2020, Molkentin et al 2017). Mechanically, the increases in collagen content, alignment, and crosslinking alter myocardial stiffness and directly impair myocardial relaxation, pump generating capacity, oxygen diffusion, and cardiac geometry (Turner et al 2019, Fedak et al 2003). These changes also weaken individual cardiomyocyte function through mechanosensing pathways and physically disrupting electrical conduction between adjacent cardiomyocytes (Perestrelo et al 2020). Unlike secondary fibrosis and ECM changes from cardiac injury, these matrix changes in inherited cardiomyopathies are gradual leading to progressive disturbances in both function and structure that in turn promote further matrix remodeling (Raman et al 2019, Cartledge et al 2015). In I61Q and L48Q mouse models, p38 knockout impairs fibroblast activation and prevents matrix remodeling, thus maintaining greater force generation and systolic function of both the muscle and cardiomyocyte. In contrast, the activation of p38 could account for the diastolic dysfunction observed in this study by increased myocardial stiffness. While EDPVR, a measure of passive stiffness, was not altered and the total percent fibrosis was relatively low overall, *ex-vivo* studies of decellularized cardiac tissue can further examine this question (Figure 4, 7). Indeed, recent studies in inbred I61Q mice elucidated increased whole heart stiffness and fiber alignment via these methods (unpublished data). Overall, the importance of the fibroblast p38-MAPK in mediating the ECM that influence cardiac remodeling is highlighted in studies that demonstrate the effectiveness of p38 inhibitors as therapeutic avenues of preventing this remodeling (Marber et al 2011). It was previously thought that the modulating the p38-MAPK pathway in the cardiomyocyte itself accounted for

these changes; however, the results from targeted studies within the cardiomyocyte are variable (Turner et al 2019, Nishida et al 2004, Braz et al 2003). Therefore, research has focused on the fibroblast p38-MAPK and subsequent matrix effects on this cardiac remodeling mostly in cardiac injury models (Turner et al 2019). This study, however, demonstrates that the targeted approach to alter the matrix by way of fibroblast p38 offers an ECM mechanism behind cardiac remodeling in inherited cardiomyopathies as well (Turner et al 2019).

Based on these changes to whole heart phenotype, the cardiomyocyte was evaluated to test the hypothesis that matrix remodeling was impacting individual cardiomyocyte function and contractility. p38 knockout in the fibroblast was demonstrated to rescue contractile characteristics of the cardiomyocyte as quantified by two key metrics, sarcomere length and intracellular Ca^{2+} (Figure 3). Interestingly, manipulating intracellular Ca^{2+} levels in the myocyte by modulation of the Ca^{2+} transporter SERCA has already been demonstrated to alter whole heart DCM phenotype *in-vivo* in I61Q mice (Davis et al 2016). So how then does modifying the matrix through the fibroblast also result in this change of Ca^{2+} handling to improve contractility? Various mechanisms via the ECM and even the fibroblast itself alter Ca^{2+} handling in the cardiomyocyte. Mechanosensing machinery in the cardiomyocyte, such as through integrins, cadherins, ion channels, and the cytoskeleton, sense matrix mechanical changes that in turn can modulate Ca^{2+} handling kinetics (Ward et al 2020, Herum et al 2017). Indeed, *in-vitro* studies have demonstrated that cardiomyocytes grown on varying substrate stiffness exhibit changes to their Ca^{2+} transients through altered SERCA expression and Ca^{2+} channel currents (Sewanan et al 2019, Jacot et al 2008). Another potential mechanism for altered Ca^{2+} handling is direct biochemical signaling in from the fibroblast itself. There are many proposed mechanisms of

fibroblast-cardiomyocyte crosstalk such as paracrine signaling, gap junctions, and newly discovered nanotubules that can directly and indirectly influence myocyte Ca^{2+} handling (Cartledge et al 2015, Hilal-Dandan 2009, Hall et al 2021). For example, in co-culture with activated fibroblasts, but not quiescent fibroblasts, Ca^{2+} transients and SR Ca^{2+} content were negatively impacted through paracrine effects of the fibroblast on SERCA (Cartledge et al 2015, Hilal-Dandan 2009). Thus, the role of the fibroblast on matrix remodeling and in direct crosstalk with cardiomyocytes creates multiple avenues to alter cardiomyocyte function and Ca^{2+} handling, and more work is needed to investigate the specific mechanisms in these models.

It was then investigated whether this change in cardiomyocyte tension generation could be used to predict the observed alterations in whole heart phenotype. By utilizing the tension index to predict direction and magnitude of cardiac maladaptive remodeling, it was shown that this index in I61Q with fibroblast p38 knockout did correlate with the observed improvement in left ventricular dimensions but did not correlate, however, with the heart weight to body weight ratio, a metric of cardiac hypertrophy in mice. Both clinical DCM and HCM, as well as the corresponding inbred I61Q and L48Q mouse models, have been characterized by dilatative and concentric hypertrophy respectively (McKenna et al 2020, Davis et al 2016). At the cellular level, cardiomyocyte hypertrophy is characterized by addition of sarcomeres in parallel or series resulting in myocyte growth through concentric or eccentric hypertrophy respectively (Frey et al 2004). A component of the ECM that is secreted by the fibroblast, fibronectin, has been implicated as mediator of hypertrophy in a pressure-overload model (Konstandin et al 2013). The direct role of fibroblast p38-MAPK in cardiomyocyte hypertrophy has also been investigated in models of injury or drug induced cardiac hypertrophy and heart failure (Bageghni et al 2018,

Turner et al 2019) Interestingly, paracrine factors from fibroblasts implicated in inducing cardiomyocyte hypertrophy, such as fibroblast growth factor (FGF)-2, insulin-like growth factor (IGF-1), TGF-B, and IL-6 are modulated by the p38-MAPK pathway directly (Turner et al 2019). In particular, fibroblast p38 mediated production of IL-6 has been extensively studied, with the link of IL-6's role in cardiomyocyte hypertrophy *in-vitro* and *in-vivo* well established (Bageghni et al 2018, Turner et al 2019). Therefore, it can be hypothesized that modulating fibroblast p38-MAPK would have effects on cardiac hypertrophy. Heart weight to body weight ratio, however, was unchanged between all groups in this study (Figure 2,4,6,7). When this ratio was measured in mixed strain I61Q mice without tamoxifen administration, however, it was increased compared to controls mirroring the expected inbred I61Q result (Figure 1G). It is hypothesized that the tamoxifen administration could be contributing to the insensitivity of this ratio as a measure of hypertrophy in these models as this drug has already been shown to influence bone metabolism and skeletal growth (Zhong et al 2015). Thus, to further investigate the effect of fibroblast p38-MAPK and matrix remodeling on hypertrophy and confirm the predictive value of tension index in models that manipulate matrix remodeling, additional metrics, such as isolated cardiomyocyte length-width ratio and area, should be explored.

While it is intriguing that manipulation of primary resident cardiac fibroblasts via the p38-MAPK pathway can have overall effects on cardiomyopathy structural and functional phenotype, how does this clinically translate to both the human as well as veterinary patient populations? As mentioned previously, incidence of inherited cardiomyopathies ranges from 1:250-500 in the human population (Mckenna et al 2020). DCM in the canine population is the second most common acquired cardiac diseases in dogs with links to genetic loci in several breeds including

Doberman pinchers, boxers, great Danes, and other large breed dogs (Dutton et al 2018). The complexity of incomplete disease penetrance and varying clinical presentations, like in humans, is also prevalent in the canine DCM population (Dutton et al 2018). Additionally, varying environmental factors, such as diet, have been implicated in DCM disease incidence especially in suspectable breeds such as the golden retriever (Dutton et al 2018). A common histological feature of DCM for both species is the accumulation of fibrosis (Legge et al 2013, Lobo et al 2010). In contrast, inherited HCM is the most common cardiomyopathy presentation in the feline population (Fox et al 2018). Similarly to HCM in humans as well as DCM, HCM in cats is also characterized varying clinical disease presentation as well as extensive myocardial fibrosis (Kitz et al 2019). While the early pathogenesis of fibrosis and matrix remodeling has not been well studied in these DCM and HCM veterinary populations, due to the similarity to human clinical phenotype and genetic risk factors, it can be hypothesized matrix remodeling also plays a key role in these species. Early diagnosis is key for both human and veterinary populations to improve clinical outcome (Schultheiss et al 2019). Especially for veterinary patients, clinical diagnosis is often made late in the disease course and biomarkers such prohormones from myocardium stress or stretch, such as NT-proBNP, are more sensitive for severe disease (Hsu et al 2009, Gavazza et al 2020). If matrix remodeling and early fibrotic indicators do play a role in early disease progression, serum fibrosis biomarkers, such as procollagen type III, connective tissue growth factor (CTGF), MMP-2, MMP-9, and TIMP-1 which have been shown to be increased in human DCM patients even without detectable fibrosis, could provide a useful clinical screening tools for both humans and veterinary patients in combination with genetic screening (Eijgenraam et al 2020). Additionally, non-invasive imaging modalities, such as magnetic resonance elastography (MRE) and ultrasound cardiac shearwave elastography (SWE)

could be used in both human and veterinary patients to detect changes in cardiac stiffness early in the disease process (Ward et al 2020).

Even with the current understanding of the complexity and genetic associations with inherited cardiomyopathies, mainstay therapies for HCM and DCM still represent palliative efforts to maintain cardiac function and hemodynamics particularly through the end stages of clinical disease (Greenberg et al 2021). The p38-MAPK pathway has been a topic of discussion for therapeutic intervention of heart disease, particularly in targeting the pathway within cardiomyocytes themselves (Arabacilar et al 2015). Currently, a p38 inhibitor, ARRY-371797, is in clinical trials for patients with inherited cardiomyopathies (Reichardt et al 2021, NCT03439514). The current p38 inhibitors available, however, are global inhibitors and can lead to unwanted side effects due to due to the ubiquitous nature of p38 in various tissues (Arabacilar et al 2015). Cell-selective p38 therapeutic targets were previously thought to be unrealistic; however, engineered T-cell technology has been shown to selectively target pathological cardiac fibroblasts by the fibroblast activation protein (FAP) antigen to reduce cardiac fibrosis and rescue of cardiac function after injury (Aghajanian et al 2019). This technology could be applied to future studies to selectively target activated fibroblasts or prevent fibroblast activation early in the disease process through p38 or its downstream targets, ECM composition, or paracrine and direct mediators. The timing of when to inhibit fibroblast activation and its effects is important to consider. One study by Meng et al in 2018 found that selectively abating activation cardiac fibroblasts early in the disease process of a mouse model of inherited HCM not only preserved cardiac function and prolonged lifespan but also rescued the cardiac hypertrophy phenotype. If ablated late in the disease process, however, this rescue of hypertrophy was not observed.

Further studies in I61Q and L48Q mouse models are needed to determine the optimal time point of matrix remodeling modulation to achieve therapeutic goals in these models and provide insight on clinically relevant therapeutic windows in patients. A balance, however, is needed between targeting the fibroblast p38-MAPK pathway without inhibiting the key role fibroblasts play in adaptive remodeling and maintaining appropriate cardiac structure (Czubryt 2019, Reichardt et al 2021). Further work is also needed to evaluate the efficacy of modulating fibroblast p38-MAPK on other *in-vivo* models of inherited DCM and HCM such as in mutations more commonly observed in the human and veterinary populations.

Overall, this study demonstrates how the modulating the ECM through the fibroblast in inherited cardiomyopathies can directly affect phenotype at the whole heart and individual cardiomyocyte level and offer insights into early diagnostic tools and targeted therapeutic approaches.

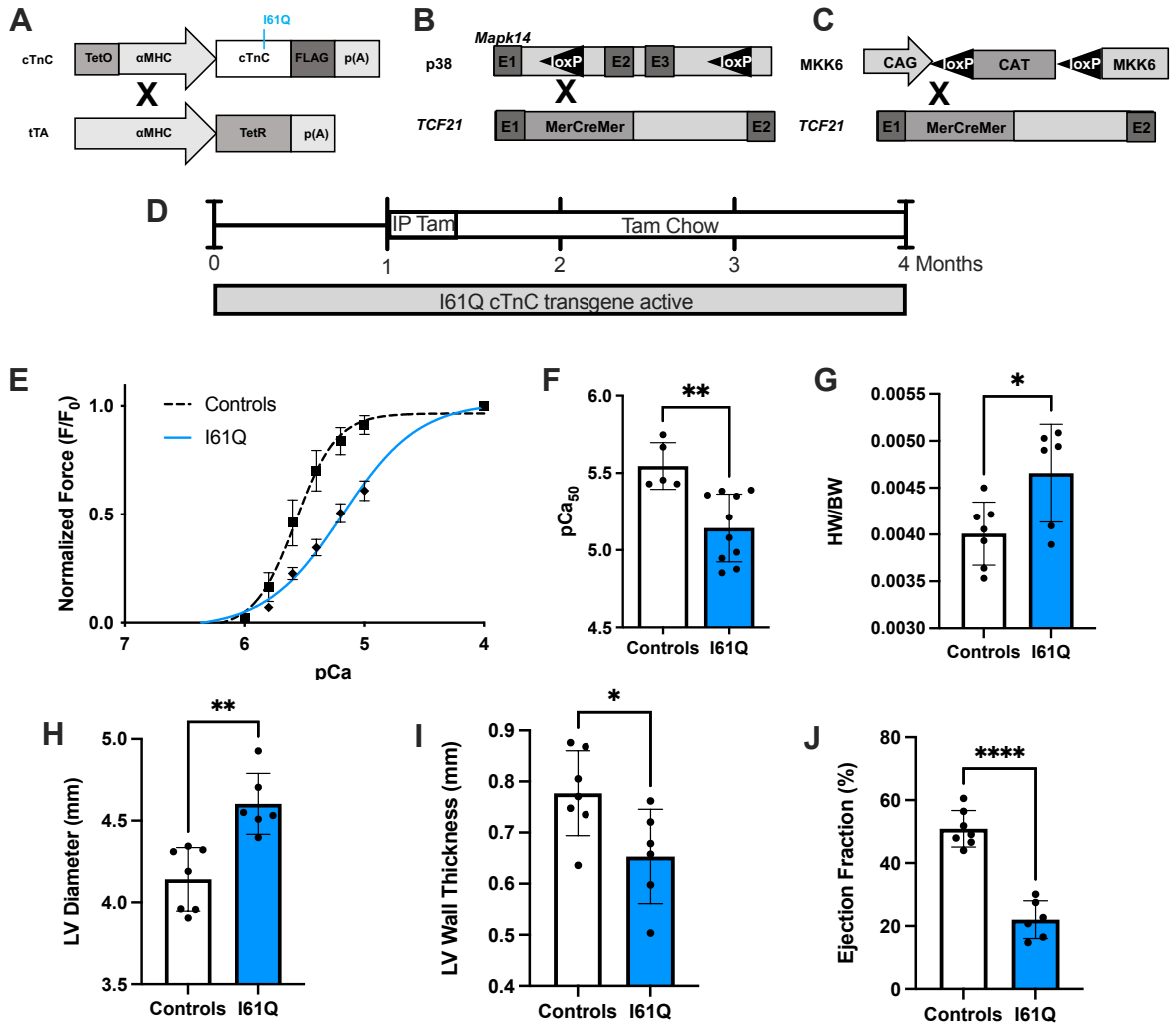

Figure 1. Mixed-strain I61Q mice demonstrate reduced calcium sensitivity of tension generation and DCM phenotype

(A) Schematic depiction of the bi-transgenic system for cardiac specific expression via alpha myosin heavy chain promoter (αMHC) of WT and I61Q cTnC with a carboxy-terminal Flag epitope. tTA is the tetracycline transactivator construct, TetR is the tetracycline repressor, and TetO is the tetracycline operator. Schematic depiction of the (B) *Mapk14* loxP targeted allele for inactivation after Cre-dependent recombination, (C) MKK6 loxP dependent transgene, and (B-C) *Tcf21* locus with MerCreMer cDNA that is tamoxifen regulated. (D) Schematic of tamoxifen dosing scheme with 5 days of IP tamoxifen and maintained on tamoxifen chow until 4 months of age. Grey bar represents I61Q cTnC transgene activation. (E-F) Ca^{2+} sensitivity of tension generation for I61Q demembranated cardiac muscle compared to controls by (E) normalized force-pCa^{2+} curve and (F) pCa_{50}, n=2-3 with 2-3 measurements per mouse. (G) Average HW/BW in controls and I61Q mice without tamoxifen, n=6-7. (H-J) Average left ventricular diastolic diameter, (I) left ventricular wall thickness, and (J) ejection fraction measured by M-mode echocardiography in controls and I61Q mice without tamoxifen, n=6-7. Mean+SD; * P<0.05; **P<0.01, ****P<0.0001; unpaired t test

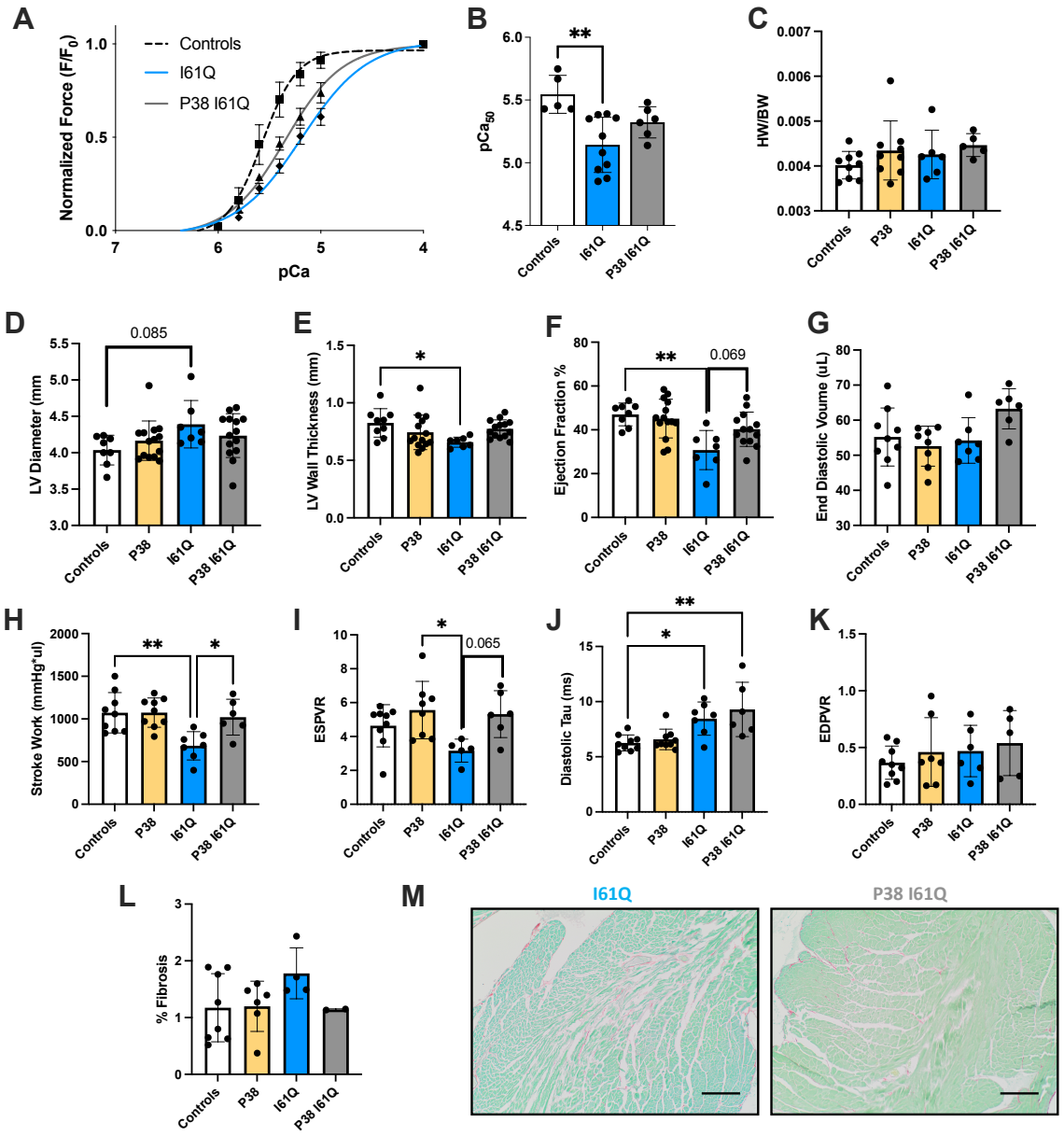

Figure 2. Loss of fibroblast p38 rescues I61Q DCM dilated phenotype, systolic dysfunction, and impaired contractility while maintaining reduced I61Q Ca^{2+} sensitivity of tension generation

(A-B) Effects of fibroblast p38 knockout on I61Q Ca^{2+} sensitivity of tension generation by (A) normalized force-pCa^{2+} curve and (B) pCa_{50} n=2-3 with 2-3 measurements per mouse. (C) Average HW/BW at 4 months of age in controls, P38, I61Q, and P38 I61Q mice; n=5-9. (D-F) Average left ventricular diastolic diameter, (E) left ventricular wall thickness, and (F) ejection fraction at 4 months of age measured via echocardiography M-mode in controls, P38, I61Q, and P38 I61Q mice; n=7-14. (G-L) Average end diastolic volume, (H) stroke work, (I) end systolic pressure volume relationship (ESPVR), (J) isovolumic relaxation constant (Tau), and (K) end diastolic pressure volume relationship (EDPVR) measured via pressure-volume loops at 4 months of age in controls, P38, I61Q, and P38 I61Q mice; n=5-8. (L) Quantification and (M) pico-sirus red stained histological images at 10x from hearts of controls, P38, I61Q, and P38 I61Q at 4 months of age. Red staining indicates fibrosis. n=2-8. Scale bar = 100um.

Mean+SD; * P<0.05; **P<0.01; one-way ANOVA

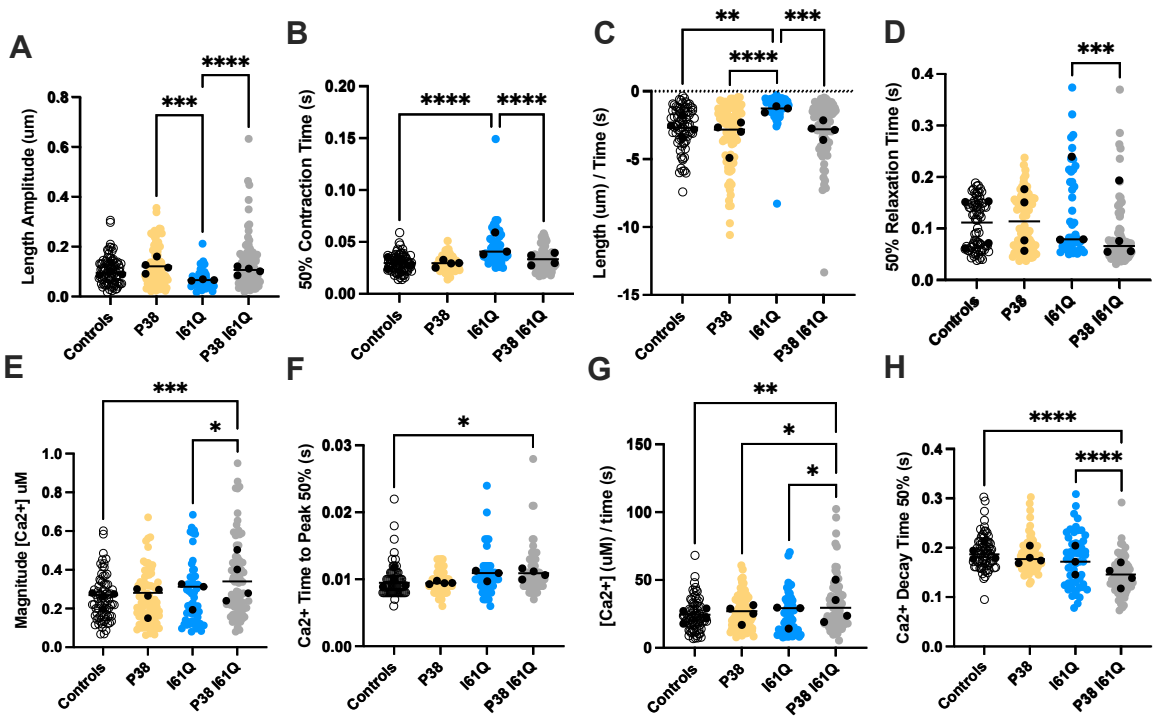

Figure 3. Loss of fibroblast p38 improves I61Q myocyte mechanics by altered Ca^{2+} handling
(A-D) Average myocyte shortening, (B) 50% contraction time, (C) maximal rate of change during the contraction, and (D) 50% relaxation time of isolated myocytes from controls, p38, I61Q, and p38 I61Q hearts; n=>60 myocytes distributed across 3-4 preparations per group. (E-H) Ca^{2+} amplitude, (F) 50% Ca^{2+} transient amplitude time, (G) maximal rate of change during Ca^{2+} release, and (H) 50% Ca^{2+} transient decay time of isolated myocytes after Fura-2 incubation from controls, p38, I61Q, and p38 I61Q mice; n=>40 myocytes distributed across 3-4 preparations per group.
Mean with individual data; * P<0.05; **P<0.01; ***P<0.001; ****P<0.0001; one-way ANOVA

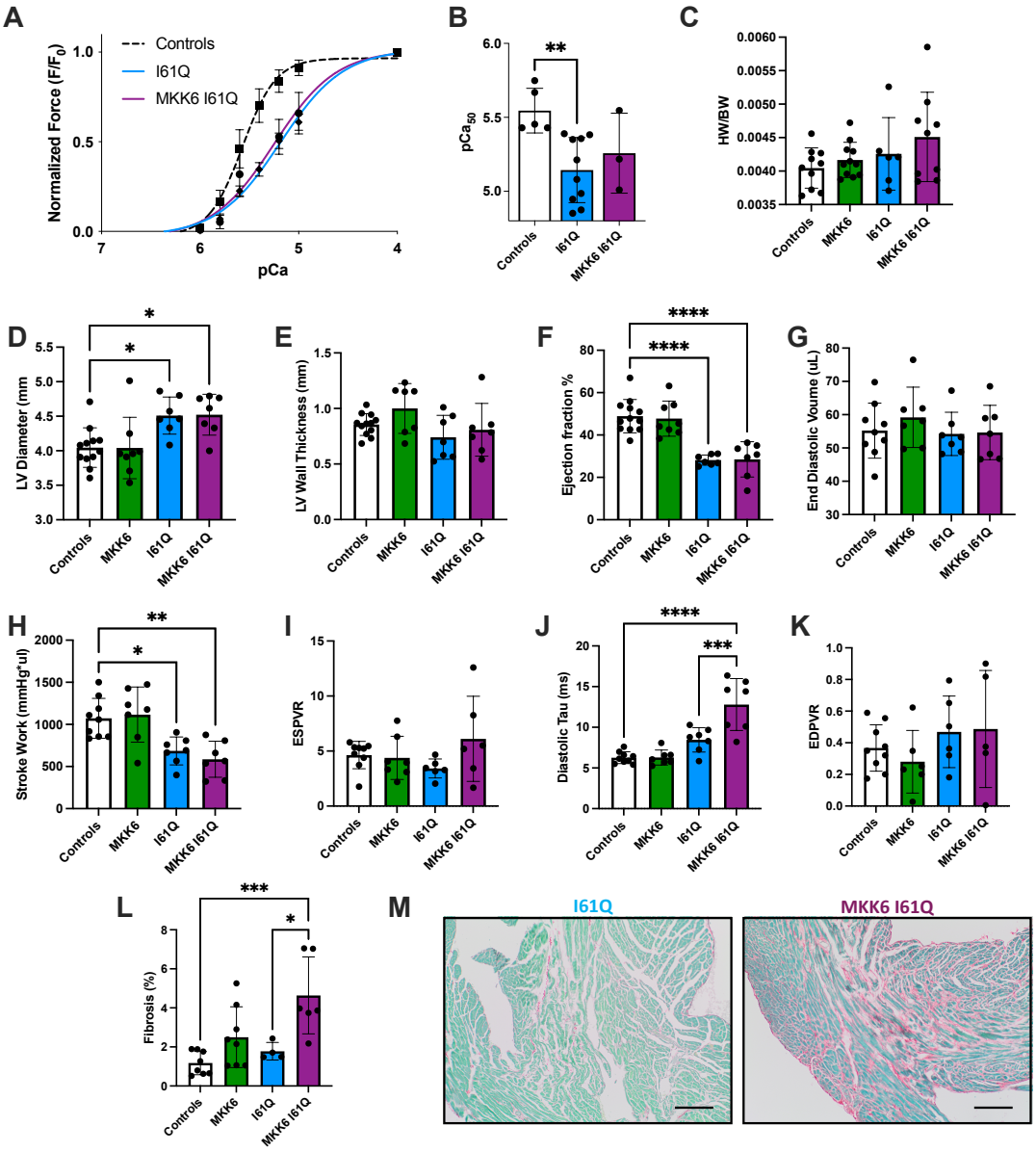

Figure 4. Fibroblast p38 activation increases fibrosis but does not alter I61Q DCM Ca^{2+} sensitivity of tension generation, ventricular chamber dilation, or systolic dysfunction

(A-B) Effects of fibroblast MKK6 activation on I61Q Ca^{2+} sensitivity of tension generation by (A) normalized force-pCa^{2+} curve, and (B) pCa_{50}, n=1-3 with 2-3 measurements per mouse. (C) Average HW/BW at 4 months of age in controls, MKK6, I61Q, and MKK6 I61Q mice; n=5-9. (D-F) Average left ventricular diastolic diameter, (E) left ventricular wall thickness, and (F) ejection fraction at and 4 months of age via echocardiography M-mode in controls, MKK6, I61Q, and MKK6 I61Q mice; n=8. (G-L) Average end diastolic volume, (H) stroke work, (I) end systolic pressure volume relationship (ESPVR), (J) isovolumic relaxation constant (Tau), and (K) end diastolic pressure volume relationship (EDPVR) via pressure-volume loops at 4 months of age in controls, MKK6, I61Q, and MKK6 I61Q mice; n=5-8. (L) Quantification and (M) pico-sirus red stained histological images at 10x from hearts of controls, MKK6, I61Q, and MKK6 I61Q at 4 months of age. Red staining indicates fibrosis. n=4-8. Scale bar = 100um.

Mean+SD; * P<0.05; **P<0.01, ***<0.0001, ****P<0.0001, one-way ANOVA

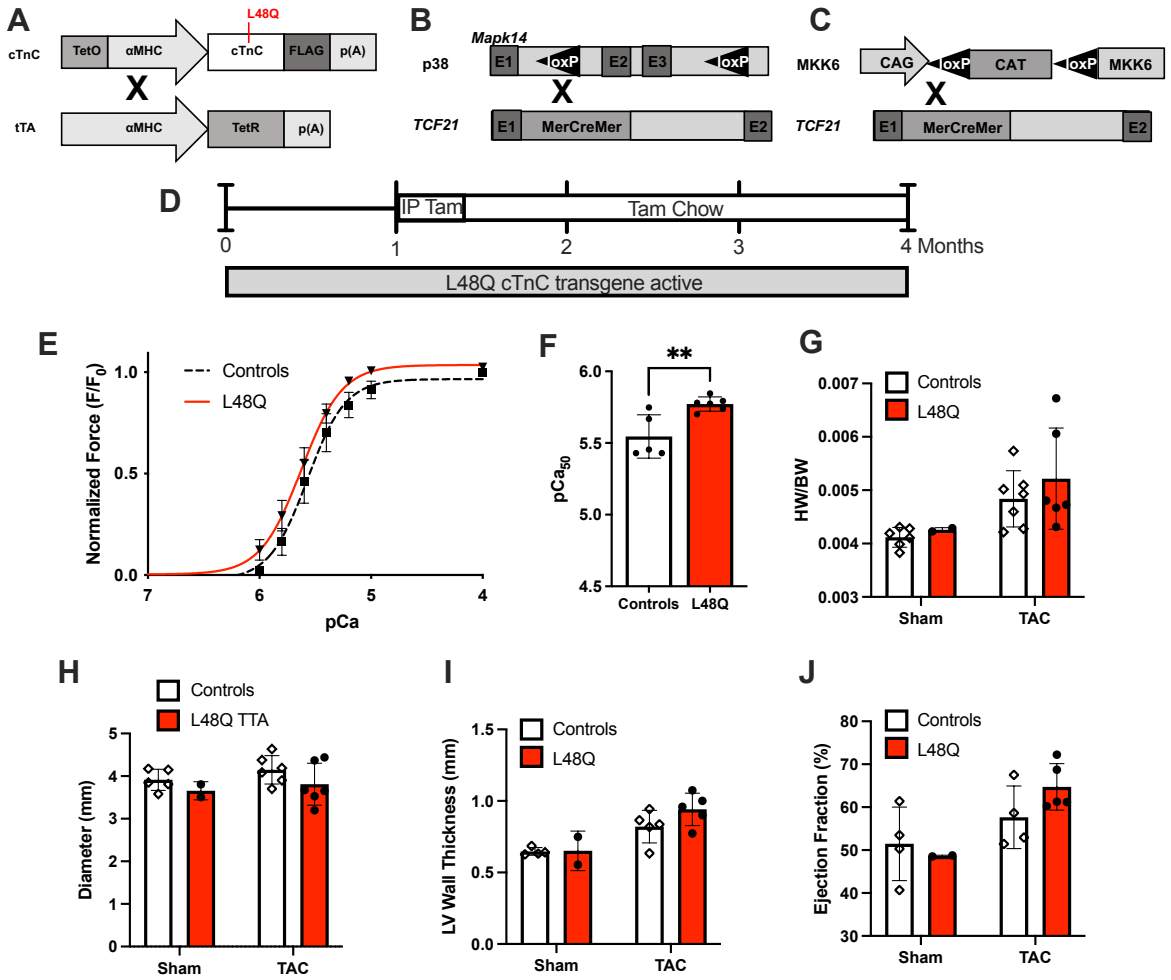

Figure 5. Mixed strain L48Q mice have enhanced Ca^{2+} sensitivity of tension generation and may demonstrate HCM phenotype after TAC

(A) Schematic depiction of the bi-transgenic system for cardiac specific expression via alpha myosin heavy chain promoter (αMHC) of WT and L48Q cTnC with a carboxy-terminal Flag epitope. tTA is the tetracycline transactivator construct, TetR is the tetracycline repressor, and TetO is the tetracycline operator. Schematic depiction of the (B) *Mapk14* loxP targeted allele for inactivation after Cre-dependent recombination, (C) MKK6 loxP dependent transgene, and (B-C) *Tcf21* locus with MerCreMer cDNA that is tamoxifen regulated. (D) Schematic of tamoxifen dosing scheme with 5 days of IP tamoxifen and maintained on tamoxifen chow until 4 months of age. Grey bar represents L48Q cTnC transgene activation. (E-F) Ca^{2+} sensitivity of tension generation for L48Q demembranated cardiac muscle compared to controls by (E) normalized force-pCa^{2+} curve and (F) pCa_{50}, n=2-3 with 2-3 measurements per mouse. (G-J) The effect of TAC or sham procedure in controls and L48Q mice by average (G) HW/BW, (H) left ventricular diameter, (I) left ventricular wall thickness, and (J) ejection fraction, Sham n=2-5, TAC n=6.

Mean+SD; ** P<0.01; unpaired t test

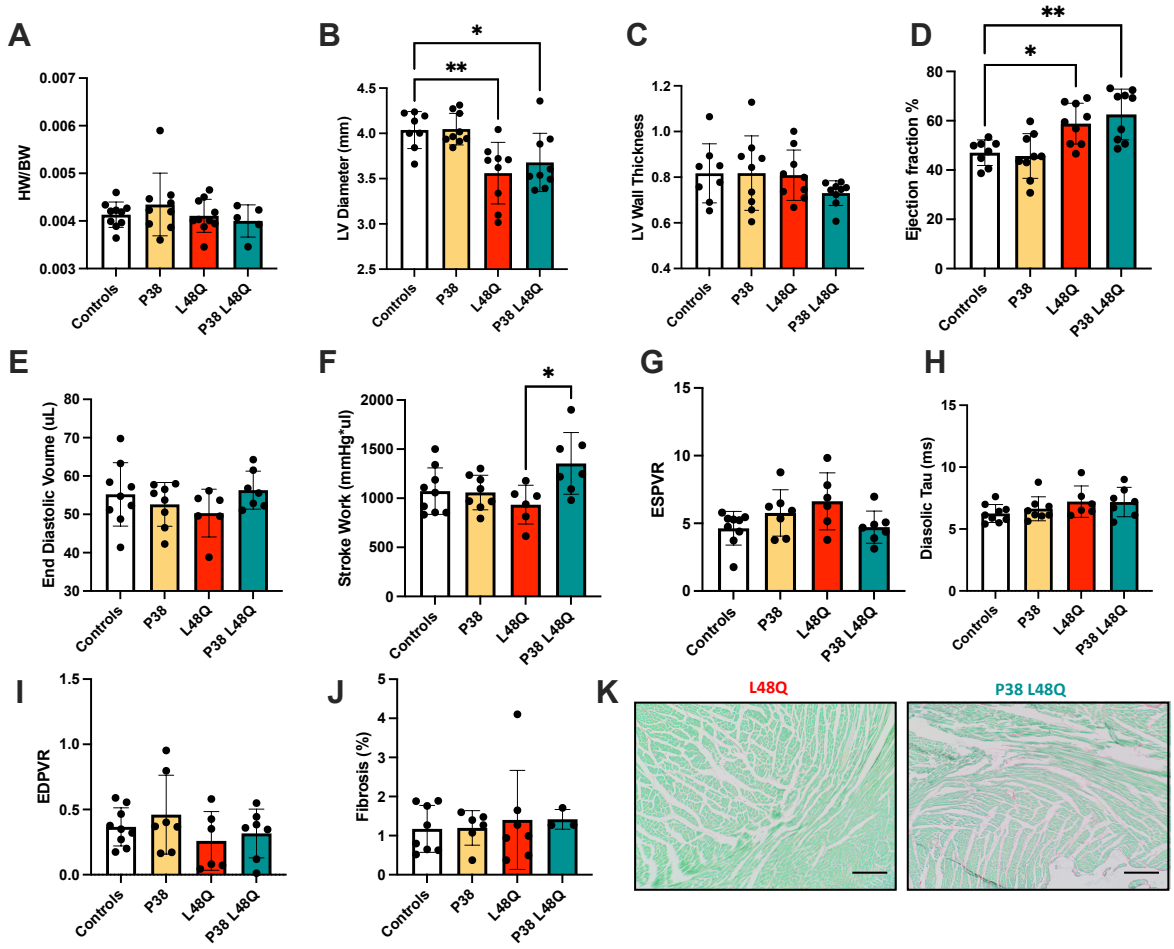

Figure 6. Loss of fibroblast p38 enhances L48Q stroke work but does not alter reduced ventricular diameter or enhanced ejection fraction

(A) Average HW/BW at 4 months of age in controls, p38, L48Q, and p38 L48Q mice; n=6-9. (B-D) Average left ventricular diastolic diameter, (C) left ventricular wall thickness, and (D) ejection fraction at 4 months of age measured via echocardiography M-mode in controls, p38, L48Q, and p38 L48Q mice; n=8-9. (E-I) Average end diastolic volume, (F) stroke work, (G) end systolic pressure volume relationship (H) isovolumic relaxation constant (Tau), and (I) end diastolic pressure volume relationship measured via pressure-volume loops at 4 months of age in controls, p38, L48Q, and p38 L48Q mice; n=6-9. (J) Quantification and (K) pico-sirus red stained histological images from hearts of controls, p38, L48Q, and p38 L48Q at 4 months of age. Red staining indicates fibrosis. n=3-8. Scale Bars =100um.

Mean+SD; * P<0.05; **P<0.01; one-way ANOVA

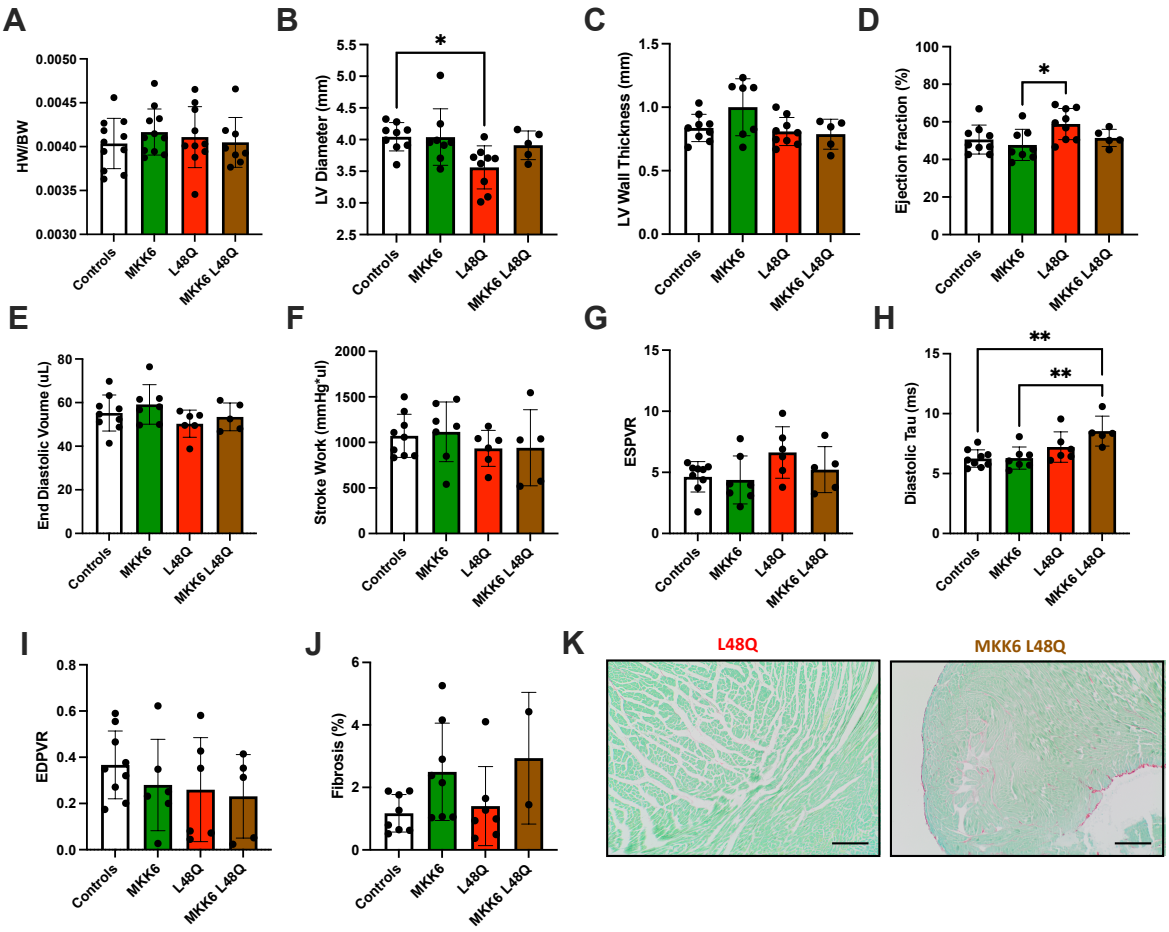

Figure 7. Fibroblast p38 activation impairs L48Q diastolic function and rescues reduced diameter and hyper-dynamic systolic function

(A) Average HW/BW at 4 months of age in controls, MKK6, L48Q, and MKK6 L48Q mice; n=9. (B-D) Average left ventricular diastolic diameter, (C) left ventricular wall thickness, and (D) ejection fraction at 4 months of age measured via echocardiography M-mode in controls, MKK6, L48Q, and MKK6 L48Q mice; n=5-9. (E-I) Average end diastolic volume, (F) stroke work, (G) end systolic pressure volume relationship (H) isovolumic relaxation constant (Tau), and (I) end diastolic pressure volume relationship measured via pressure-volume loops at 4 months of age in controls, MKK6, L48Q, and MKK6 L48Q mice; n=5-9. (I) Quantification and (J) pico-sirus red stained histological images from hearts of controls, MKK6, L48Q, and MKK6 L48Q at 4 months of age. Red staining indicates fibrosis. n=2-8. Scale Bars = 100um.

Mean+SD; * P<0.05, ** P<0.01; one-way ANOVA

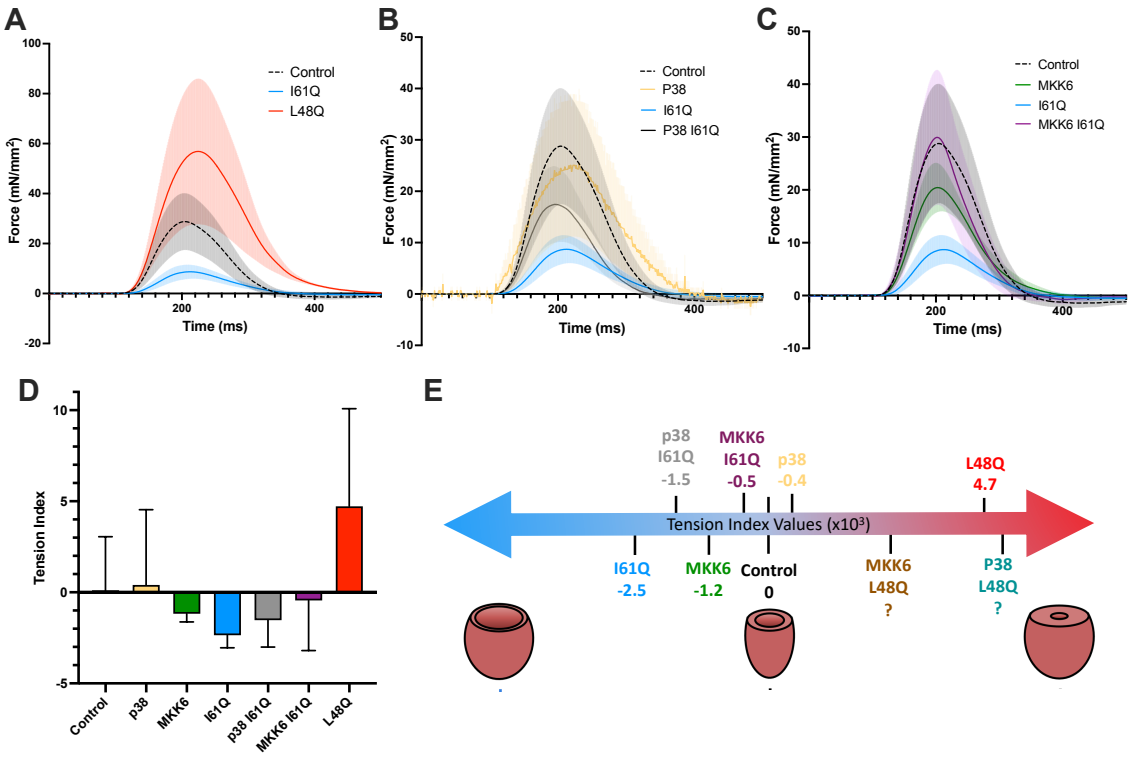

Figure 8. Manipulation of fibroblast p38-MAPK pathway alters I61Q predictive tension index
(A) Mean twitch force over time of controls (black, dashed), I61Q (blue), and L48Q (red) in intact muscle strips, n=2-4, Mean curve+SD. (B) Mean twitch force over time of controls (black, dashed), P38 (yellow), I61Q (blue), and P38 I61Q (grey) in intact muscle strips, n=2-4, Mean curve+SD (C) Mean twitch force over time of controls (black, dashed), MKK6 (green), I61Q (blue), and MKK6 I61Q (purple) in intact muscle strips, n=2-4, Mean curve+SD (D) Tension index values normalized to controls for P38, MKK6, I61Q, P38 I61Q, MKK6 I61Q, and L48Q n=2-4, mean+SD. (E) Tension index values demonstrating the magnitude and direction of dilated growth relative to controls for P38, MKK6, I61Q, P38 I61Q, MKK6 I61Q, and L48Q including hypothesized tension index values for P38 L48Q and MKK6 L48Q.

Echo Parameter:	NTG	TTA	TCF21	P38F/F	P Value
HR (bpm)	412.13 ±26.16	396.89 ±29.79	423.56 ±21.54	397.96 ±17.31	0.48
IVRT (ms)	17.76 ±1.23	17.44 ±1.92	19.79 ±3.07	18.54 ±2.2	0.23
IVCT (ms)	17.31 ±3.28	16.24 ±2.59	16.18 ±2.35	17.04 ±1.54	0.54
SV (µL)	32.4 ±4	37.28 ±7.77	33.13 ±7.02	32.93 ±7.1	0.22
EF (%)	47.15 ±6.72	48.5 ±7.62	42.9 ±11.26	46.36 ±6.73	0.76
E/A	2.53 ±0.73	3 ±1.46	3.39 ±2.41	2.67 ±0.88	0.71
E/e'	34.56 ±7.9	34.01 ±9.15	39.47 ±11.53	33.59 ±4.84	0.7
LV Diameter (mm)	3.99 ±0.35	4.16 ±0.28	4.27 ±0.21	4.01 ±0.25	0.21
LV Wall Thickness (mm)	0.88 ±0.12	0.81 ±0.14	0.84 ±0.08	0.89 ±0.31	0.96

Supp Table 1. No difference between control groups
Average echocardiography parameters and P values for controls with genotypes non-transgenic (NTG), tetracycline transactivator (TTA), TCF21+/-, and P38F/F 4 months of age. Heart rate (HR), stroke volume (SV), ejection fraction (EF), left ventricular diameter, and left ventricular wall thickness were measured via M-mode. Isovolumetric relaxation (IVRT) and contraction (IVCT), E/A, and E/e' were measured via pulse wave and tissue doppler. No P-value was <0.05. n=5-9, mean ±SD, One-way ANOVA

PV Loop Parameter:	Controls (C)	P38 (P)	I61Q (I)	P38 I61Q (PI)	P Value	Sig Comparisons
HR (bpm)	470.4 ±24.5	457 ± 25.3	459.8 ± 25	450 ± 23.7	ns	
SW (mmHg*µL)	1072.5 ± 236.4	1059.8 ±165.9	685 ± 165.9	1021.1 ± 209.8	0.002	C-I, P-I, I-PI
SV (µL)	11.9 ± 3	12.1 ± 2.5	8.6 ± 1.8 #	11.2 ± 1.8	0.03	P-I
Vmax (µL)	55.9 ± 8.2	53.4 ± 5.6	55.2 ± 7.1	63.8 ± 6.1	ns	
Ves (µL)	44 ±6.6	41.4 ± 4.1	46.8 ± 6.1	52.9 ± 7.3	0.02	P-PI
Ved (µL)	55.2 ±8.3	52.6 ± 5.3	54.2 ± 6.5	63.3 ± 5.7	0.04	P-PI
Pmax (mmHg)	104.2 ±12.2	101.7 ± 10.3	97.5 ± 8.4	108 ± 15.2	ns	
Pes (mmHg)	103.6 ±12.2	100.9 ± 10.6	97.1 ± 8.2	107.4 ± 15.2	ns	
Ped (mmHg)	6.1 ±2.8	5.3 ± 1	6.4 ± 5	8.8 ±7	ns	
dP/dtmax (mmHg/s)	10148.2 ±2424.7	10052.3 ± 1535.4	6922.6 ± 1309.8	6784 ± 1645.3	<0.001	C-I, C-PI, P-I, P-PI
dP/dtmin (mmHg/s)	-9889.5 ±1617.1	-10509.3 ± 1649.2	-7540.5 ± 1554.1	-6772.5 ± 1868.2	0.002	C-PI, P-I, P-PI
Diastolic Tau (ms)	6.3 ±0.7	6.3 ± 0.4	8.5 ± 1.5	9.3 ± 2.5	<0.001	C-I, C-PI, P-PI
PVA vs ESP	38.1 ±10.9	31.6 ± 8.2	31 ± 11.6	31.1 ± 5.2	ns	
PVA vs EDV	92.7 ±18.9	98.8 ± 16.8	57.2 ± 20.8	83.5 ± 13.8	0.003	C-I, P-I, P-PI
PRSW	43.3 ±13.5	52.1 ± 8.3	35.7 ± 6.4	47.8 ± 11.6	ns	
ESPVR	4.6 ±1.2	5.8 ± 1.5	3.4 ± 0.9	5.3 ± 1.4	0.03	P-I
EDPVR	0.37 ±0.1	0.48 ± 0.3	0.47 ± 0.2	0.54 ± 0.3	ns	

Supp Table 2. PV Loop values demonstrate I61Q DCM diastolic dysfunction and rescue of systolic dysfunction and contractility with p38 knockout
Average PV loop parameters for controls (C), P38 (P), I61Q (I), and P38 I61Q (PI) at 4 months of age. Average heart rate (HR), stroke work (SW), stroke volume (SV), maximum volume (Vmax), end systolic volume (Ves), end diastolic volume (Ved), maximum pressure (Pmax), end systolic pressure (Pes), end diastolic pressure (Ped), maximum rate of pressure change (dP/dtmax), minimum rate of pressure change (dP/dtmin), isovolumic relaxation constant (Tau), pressure-volume area vs end systolic pressure (PVA vs ESP), pressure-volume area vs end diastolic volume (PVA vs EDV), preload recruitable stroke work (PRSW), end systolic pressure volume relationship (ESPVR), and end diastolic pressure volume relationship (EDPVR). Significant P-values via one-way ANOVA and significant comparisons ($P<0.05$) via Tukey's multiple comparison test listed. n=5-8, mean ±SD

PV Loop Parameter:	Controls (C)	MKK6 (M)	I61Q (I)	MKK6 I61Q (MI)	P Value	Sig Comparisons
HR (bpm)	470.4 ±24.5	463 ±28.2	459.8 ± 25	452.2 ±29.4	ns	
SW (mmHg*µL)	1072.5 ± 236.4	1116.6 ±327.7	685 ± 165.9	586.2 ±214	<0.001	C-I, C-MI, M-I, M-MI
SV (µL)	11.9 ± 3	13.5 ±4.7	8.6 ± 1.8 #	8.8 ±3.3	0.03	M-I (P =0.05)
Vmax (µL)	55.9 ± 8.2	59.8 ±8.9	55.2 ± 7.1	55.1 ±8	ns	
Ves (µL)	44 ±6.6	47.1 ±6	46.8 ± 6.1	47.4 ±8.2	ns	
Ved (µL)	55.2 ±8.3	59.2 ±9.1	54.2 ± 6.5	54.7 ± 8.2	ns	
Pmax (mmHg)	104.2 ±12.2	98.3 ±7.9	97.5 ± 8.4	90.9 ±10	ns	
Pes (mmHg)	103.6 ±12.2	97.6 ±7.9	97.1 ± 8.2	90.5 ±10.2	ns	
Ped (mmHg)	6.1 ±2.8	5.3 ±1.1	6.4 ± 5	10.7 ±1.1	0.008	C-MI, M-MI
dP/dtmax (mmHg/s)	10148.2 ±2424.7	9540.7 ±1826.2	6922.6 ± 1309.8	5362.1 ±1153.3	<0.001	C-I, C-MI, M-MI
dP/dtmin (mmHg/s)	-9889.5 ±1617.1	-9407.6 ±1916.9	-7540.5 ± 1554.1	-4816.5 ±1562.6	<0.001	C-I, C-MI, M-MI, I-MI
Diastolic Tau (ms)	6.3 ±0.7	6.3 ±0.9	8.5 ± 1.5	12.8 ±3.2	<0.001	C-MI, M-MI, I-MI
PVA vs ESP	38.1 ±10.9	46.8 ±26.8	31 ± 11.6	55.7 ±31.9	ns	
PVA vs EDV	92.7 ±18.9	84 ±14.4	57.2 ± 20.8	65.4 ±30.9	0.03	C-I
PRSW	43.3 ±13.5	47.7 ±16.8	35.7 ± 6.4	36.4 ±16.8	ns	
ESPVR	4.6 ±1.2	4.4 ±2	3.4 ± 0.9	6.1 ±3.9	ns	
EDPVR	0.37 ±0.1	0.28 ±0.2	0.47 ± 0.2	0.49 ±0.4	ns	

Supp Table 3. PV Loop values for demonstrate I61Q DCM impaired diastolic dysfunction and unaltered systolic function with p38 activation
Average PV loop parameters for controls (C), MKK6 (M), I61Q (I), and MKK6 I61Q (MI) at 4 months of age. Average heart rate (HR), stroke work (SW), stroke volume (SV), maximum volume (Vmax), end systolic volume (Ves), end diastolic volume (Ved), maximum pressure (Pmax), end systolic pressure (Pes), end diastolic pressure (Ped), maximum rate of pressure change (dP/dtmax), minimum rate of pressure change (dP/dtmin), isovolumic relaxation constant (Tau), pressure-volume area vs end systolic pressure (PVA vs ESP), pressure-volume area vs end diastolic volume (PVA vs EDV), preload recruitable stroke work (PRSW), end systolic pressure volume relationship (ESPVR), and end diastolic pressure volume relationship (EDPVR). Significant P-values via one-way ANOVA and significant comparisons ($P<0.05$) via Tukey's multiple comparison test listed. n=5-8, mean ±SD

PV Loop Parameter:	Controls (C)	P38 (P)	L48Q (L)	P38 L48Q (PL)	P Value	Sig Comparisons
HR (bpm)	470.4 ±24.5	457 ± 25.3	454.4 ±20.6	445.7 ±29.8	ns	
SW (mmHg*µL)	1072.5 ± 236.4	1059.8 ±165.9	934.9 ±197.5	1354.8 ±314.5	0.02	L-PL
SV (µL)	11.9 ± 3	12.1 ± 2.5	10.3 ±1.8	14 ±3.2	ns	
Vmax (µL)	55.9 ± 8.2	53.4 ± 5.6	51.2 ±6.1	57 ±5.2	ns	
Ves (µL)	44 ±6.6	41.4 ± 4.1	41.3 ±7.1	42.6 ±3.1	ns	
Ved (µL)	55.2 ±8.3	52.6 ± 5.3	50.3 ±6.2	56.3 ±5	ns	
Pmax (mmHg)	104.2 ±12.2	101.7 ± 10.3	107 ±1.9	110.7 ±9.2	ns	
Pes (mmHg)	103.6 ±12.2	100.9 ± 10.6	106.2 ±1.8	109.6 ±9.2	ns	
Ped (mmHg)	6.1 ±2.8	5.3 ± 1	5.4 ±1.5	7.4 ±3.8	ns	
dP/dtmax (mmHg/s)	10148.2 ±2424.7	10052.3 ± 1535.4	11152.8 ±903.2	11541.6 ±1065.7	ns	
dP/dtmin (mmHg/s)	-9889.5 ±1617.1	-10509.3 ± 1649.2	-10540.8 ±1358.3	-10612.8 ±1857.3	ns	
Diastolic Tau (ms)	6.3 ±0.7	6.3 ± 0.4	7.2 ±1.3	7.2 ±1.2	ns	
PVA vs ESP	38.1 ±10.9	31.6 ± 8.2	28.6 ±8.9	29.5 ±13.1	ns	
PVA vs EDV	92.7 ±18.9	98.8 ± 16.8	104.4 ±19.8	98.9 ±26.8	ns	
PRSW	43.3 ±13.5	52.1 ± 8.3	53 ±13.6	49.2 ±13.6	ns	
ESPVR	4.6 ±1.2	5.8 ± 1.5	6.6 ±2.1	4.7 ±1.2	0.08	
EDPVR	0.37 ±0.1	0.48 ± 0.3	0.24 ±0.2	0.32 ±0.2	ns	

Supp Table 4. PV Loop values demonstrate enhanced L48Q HCM systolic function with p38 knockout
Average PV loop parameters for controls (C), P38 (P), L48Q (L), and P38 L48Q (PL) at 4 months of age. Average heart rate (HR), stroke work (SW), stroke volume (SV), maximum volume (Vmax), end systolic volume (Ves), end diastolic volume (Ved), maximum pressure (Pmax), end systolic pressure (Pes), end diastolic pressure (Ped), maximum rate of pressure change (dP/dtmax), minimum rate of pressure change (dP/dtmin), isovolumic relaxation constant (Tau), pressure-volume area vs end systolic pressure (PVA vs ESP), pressure-volume area vs end diastolic volume (PVA vs EDV), preload recruitable stroke work (PRSW), end systolic pressure volume relationship (ESPVR), and end diastolic pressure volume relationship (EDPVR). Significant P-values via one-way ANOVA and significant comparisons ($P<0.05$) via Tukey's multiple comparison test listed unless otherwise stated. n=6-9, mean ±SD

PV Loop Parameter:	Controls (C)	MKK6 (M)	L48Q (L)	MKK6 L48Q (ML)	P Value	Sig Comparisons
HR (bpm)	470.4 ±24.5	463 ±28.2	454.4 ±20.6	432.1 ±12.2	0.05	C-ML
SW (mmHg*µL)	1072.5 ± 236.4	1116.6 ±327.7	934.9 ±197.5	941.4 ±417.3	ns	
SV (µL)	11.9 ± 3	13.5 ±4.7	10.3 ±1.8	10.9 ±3.9	ns	
Vmax (µL)	55.9 ± 8.2	59.8 ±8.9	51.2 ±6.1	54.1 ±6.6	ns	
Ves (µL)	44 ±6.6	47.1 ±6	41.3 ±7.1	44.1 ±4	ns	
Ved (µL)	55.2 ±8.3	59.2 ±9.1	50.3 ±6.2	53.5 ±6.4	ns	
Pmax (mmHg)	104.2 ±12.2	98.3 ±7.9	107 ±1.9	101.1 ±6.5	ns	
Pes (mmHg)	103.6 ±12.2	97.6 ±7.9	106.2 ±1.8	100.4 ±6.4	ns	
Ped (mmHg)	6.1 ±2.8	5.3 ±1.1	5.4 ±1.5	9.4 ±3.7	0.02	M-ML, L-ML
dP/dtmax (mmHg/s)	10148.2 ±2424.7	9540.7 ±1826.2	11152.8 ±903.2	8278 ±1182.5	0.09	M-ML (P = 0.07)
dP/dtmin (mmHg/s)	-9889.5 ±1617.1	-9407.6 ±1916.9	-10540.8 ±1358.3	-7802.3 ±1005.7	0.05	L-ML
Diastolic Tau (ms)	6.3 ±0.7	6.3 ±0.9	7.2 ±1.3	8.5 ±1.2	0.002	C-ML, M-ML
PVA vs ESP	38.1 ±10.9	46.8 ±26.8	28.6 ±8.9	32.1 ±16.3	ns	
PVA vs EDV	92.7 ±18.9	84 ±14.4	104.4 ±19.8	97.2 ±9.5	ns	
PRSW	43.3 ±13.5	47.7 ±16.8	53 ±13.6	49.4 ±20.6	ns	
ESPVR	4.6 ±1.2	4.4 ±2	6.6 ±2.1	5.2 ±1.9	ns	
EDPVR	0.37 ±0.1	0.28 ±0.2	0.24 ±0.2	0.23 ±0.2	ns	

Supp Table 5. PV Loop values demonstrate L48Q HCM diastolic dysfunction with p38 activation
Average PV loop parameters for controls (C), MKK6 (M), L48Q (L), and MKK6 L48Q (ML) at 4 months of age. Average heart rate (HR), stroke work (SW), stroke volume (SV), maximum volume (Vmax), end systolic volume (Ves), end diastolic volume (Ved), maximum pressure (Pmax), end systolic pressure (Pes), end diastolic pressure (Ped), maximum rate of pressure change (dP/dtmax), minimum rate of pressure change (dP/dtmin), isovolumic relaxation constant (Tau), pressure-volume area vs end systolic pressure (PVA vs ESP), pressure-volume area vs end diastolic volume (PVA vs EDV), preload recruitable stroke work (PRSW), end systolic pressure volume relationship (ESPVR), and end diastolic pressure volume relationship (EDPVR). Significant P-values via one-way ANOVA and significant comparisons ($P<0.05$) via Tukey's multiple comparison test listed unless otherwise stated. n=5-9, mean ±SD

References

1. Aghajanian H, Kimura T, Rurik JG, Hancock AS, Leibowitz MS, Li L, Scholler J, Monslow J, Lo A, Han W, Wang T, Bedi K, Morley MP, Saldana RAL, Bolar NA, McDaid K, Assenmacher C, Smith CL, Wirth D, June CH, Margulies KB, Jain R, Pure E, Albelda SM, Epstein JA. Targeting cardiac fibrosis with engineered T cells. 2019; 573(7774):430-433.
2. Arabacilar P, Marber M. The case for inhibiting p38 mitogen-activated protein kinase in heart failure. *Front Pharmacol* 2015 May 12;6:102.
3. Bageghni SA, Hemmings KE, Zava N, Denton CP, Porter KE, Ainscough JFX, Drinkhall MJ, Turner NA. Cardiac fibroblast-specific p38α MAP kinase promotes cardiac hypertrophy *via* a putative paracrine interleukin-6 signaling mechanism. 2018; 32(9):4941-4954.
4. Benavides F, Rulicke T, Prins JB, Bussell J, Scavizzi F, Cinelli P, Herault Y, Wedekind D. Genetic quality assurance and genetic monitoring of laboratory mice and rats: FELASA working group report. *Lab Animal* 2019; 54(2):135-148.
5. Bers DM. Cardiac excitation-contraction coupling. *Nature* 2002; 415:198-205.
6. Bildyug N. Extracellular Matrix in Regulation of Contractile System in Cardiomyocytes. *Int J Mol Sci*. 2019;20(20):5054.
7. Borlaug BA, Kass DA. Invasive hemodynamic assessment in heart failure. *Heart Fail Clin.* 2009; 5(2):217-228.
8. Czubryt MP. Cardiac fibroblast to myofibroblast phenotype conversion-an unexploited therapeutic target. *J Cardio Dev Dis* 2019; 6(28).
9. Davis J, Molkentin JD. Myofibroblasts: trust your heart and let fate decide. *J Mol Cell Cardiol* 2014; 0:9-18.
10. Davis J, Davis LC, Correll RN, Makarewich CA, Schwanekamp JA, Moussavi-Harami F, Wang D, York AJ, Wu H, Houser SR, Seidman CE, Seidman JG, Regnier M, Metzger JM, Wu JC, Molkentin JD. A tension based model distinguishes hypertrophic versus dilated cardiomyopathy. *Cell* 2016; 165(5):1147-1159.
11. Cartledge JE, Kane C, Dias P, Tesfom M, Clarke L, Mckee B, Ayoubi SA, Chester A, Yacoub MH, Camelliti P, Terracciano CM. Functional crosstalk between cardiac fibroblasts and adult cardiomyocytes by soluble mediators. *Cardio R.* 2015; 105:260-270.
12. Cheng Y, Regnier M. Cardiac troponin structure-function and the influence of hypertrophic cardiomyopathy associated mutations on modulation of contractility. *A Biochem Biophy* 2016; 601:11-12
13. Cinogolani OH, Kass DA. Pressue-volume relation analysis of mouse ventricular function. *Am J Physiol Heart Circ Physiol* 2011;301:H2198-2206.
14. Dornll GW, Molkentin JD. Manipulating cardiac contractility in heart failure. *Circulation* 2004; 109:150-158.
15. Dutton E, López-Alvarez J. An update on canine cardiomyopathies – is it all in the genes? *J Small Anim Pract* 2018; 59:455-464.
16. Eijgenraam TR, Sillje HHW, de Boer RA. Current understanding of fibrosis in genetic cardiomyopathies. *Trends Cardio Med* 2020; 30:353-361.
17. Fedak PWM, Altamentova SM, Weisel RD, Nili N, Ohno N, Verma S, Lee TJ, Kiani C, Mickle DAG, Strauss BH, Li RK. Matrix remodeling in experimental and human heart failure: a possible regulatory role for TIMP-3. *Am J Physio* 2003; 284(2):H626-H634.

18. Fomovsky GM, Thomopoulos S, Holmes JW. Contribution of extracellular matrix to the mechanical properties of the heart. *J Mol Cell Cardio* 2010; 48:490-496.
19. Fox, RP, Keene, BW, Lamb, K, et al. International collaborative study to assess cardiovascular risk and evaluate long-term health in cats with preclinical hypertrophic cardiomyopathy and apparently healthy cats: The REVEAL Study. *J Vet Intern Med* 2018; 32: 930– 943.
20. Frey N, Katus HA, Olson EN, Hill JA. Hypertrophy of the heart. *Circulation* 2004; 109:1580-1589.
21. Fujiu K, Nagai R. Fibroblast-mediated pathways in cardiac hypertrophy. *J Mol Cell Cardio* 2014; 70:64-73.
22. Galie PA, Khalid N, Carnahan KE, Westfall MV, Stegemann JP. Substrate stiffness affects sarcomere and costamere structure and electrophysiological function of isolated adult cardiomyocytes. *Cardio Path* 2013; 22:219-227.
23. Garfinkel AC, Seidman JG, Seidman CE. Genetic Pathogenesis of Hypertrophic and Dilated Cardiomyopathy. *Heart Fail Clin*. 2018;14(2):139-146.
24. Gavazza, A., Fruganti, A., Turinelli, V., Marchegiani, A., Spaterna, A., Tesei, B., Rossi, G., & Cerquetella, M. Canine Traditional Laboratory Tests and Cardiac Biomarkers. *Frontiers in veterinary science* 2020; 7(320):10.3389
25. Green EM, Wakimoto H, Anderson RL, Evanchik MJ, Gorham JM, Harrison BC, Henze M, Kawas R, Oslob JD, Rodriguez HM, Song Y, Wan W, Leinwand LA, Spudich JA, McDowell RS, Seidman JG, Seidman CE. A small-molecule inhibitor of sarcomere contractility suppresses hypertrophic cardiomyopathy in mice. *Science* 2016;351(6273):617-621.
26. Greenberg MJ, Tardiff JC. Complexity in genetic cardiomyopathies and new approaches for mechanism-based precision medicine. *J Gen Phys* 2021; 153(3):e202012662.
27. Hall C, Gehmlich K, Denning C, Pavlovic D. Complex relationship between cardiac fibroblasts and cardiomyocytes in health and disease. *J Am Heart Assoc* 2021; 10:e019338.
28. Herum KM, Lunde IG, McCulloch AD, Christensen G. The soft- and hard-heartedness of cardiac fibroblasts: mechanotransduction signaling pathways in fibrosis of the heart. *J Clin Med* 2017; 6(53):doi:10.3390.
29. Hilal-Dandan R, He H, Martin JL, Brunton LL, Dillmann WH. Endothelin downregulates SERCA2 gene and protein expression in adult rat ventricular myocytes: regulation by pertussis toxin-sensitive Gi protein and cAMP. *Am J Physiol Heart Circ Physiol* 2009; 296:H728-H734.
30. Ho CY, López B, Coelho-Filho OR, Lakdawala NK, Cirino AL, Jarolim P, et al. Myocardial fibrosis as an early manifestation of hypertrophic cardiomyopathy. *N Engl J Med* 2010; 363:552–63.
31. Hsu A, Kittleson MD, Paling A. Investigation into the use of plasma NT-proBNP concentration to screen for feline hypertrophic cardiomyopathy. *J Vet Cardiol* 2009; 11(1):S63-70. doi: 10.1016
32. Jacot JG, McCulloch AD, Omens JH. Substrate stiffness affects the functional maturation of neonatal rat ventricular myocytes. *Biophys J* 2008; 95:3479–87.
33. Janicki JS, Brower GL. The role of myocardial fibrillar collagen in ventricular remodeling and function. *J Card Fail*. 2002;8(6 Suppl):S319-25.

34. Junttila MJ, Holmstrom L, Pylkas K, Mantere T, Kaikkonen K, Porvari K, Kortelainen ML, Pakanen L, Kerkela R, Myerburg RJ, Huikuri HV. Primary myocardial fibrosis as an alternative phenotype pathway of inherited cardiac structural disorders. *Circ* 2018; 137:2716-2726.
35. Kalyva A, Parthenakis FI, Marketou ME, Kontaraki JE, Vardas PE. Biochemical characterization of Troponi C mutations causing hypertrophic and dilated cardiomyopathies. *J Muscle Res Cell Motil* 2014; 35:161-178.
36. Kapelko VI. Extracellular matrix alterations in cardiomyopathy: the possible crucial role in the dilative form. *Exp Clin Cardiol* 2001; 6(1):41-49.
37. Kashyap, R., Mittal, B. R., Manohar, K., Bhattacharya, A., & Bahl, A. Left ventricular diastolic parameters in dilated cardiomyopathy: are we missing out on something? *World J Nuc Med* 2014; *13*(2):85–87.
38. Karaahmet T, Tigen K, Dundar C, Pala S, Guler A, Kilicgedik A, Cevik C, Mahmutyazicioglu K, Isiklar I, Basaran Y. The effect of cardiac fibrosis on left ventricular remodeling, diastolic function, and N-terminal pro-B-type natriuretic peptide levels in patients with nonischemic dilated cardiomyopathy. *Echo* 2010; 27(8):954-960.
39. Kim JB, Porreca GJ, Song L, Greenway SC, Gorham JM, Church GM, et al. Polony multiplex analysis of gene expression (pmage) in mouse hypertrophic cardiomyopathy. *Science* 2007; 316:1481–4.
40. Kitz S, Fonfara S, Hahn S, Hetzel U, Kipar A. Feline hypertrophic cardiomyopathy: the consequence of cardiomyocyte-initated and macrophage-driven remodeling. *Vet Path* 2019; 56(4):565-575.
41. Konstandin MH, et al. Fibronectin contributes to pathological cardiac hypertrophy but not physiological growth. *Basic Res Cardiol.* 2013;108(5):375
42. Kreutziger KL, Piroddi N, McMichael JT, Tesi C, Poggesi C, Regnier M. Calcium binding kinetics of troponin C strongly modulate cooperative activation and tension kinetics in cardiac muscle. *J Mol Cell Cardiol* 2011; 50:165-174.
43. Legge CH, López A, Hanna P, Côté E, Hare E, Martinson SA. Histological characterization of dilated cardiomyopathy in the juvenile toy Manchester terrier. *Vet Pathol* 2013; 50(6):1043-52
44. Leite-Moreira AF. Current perspectives in diastolic dysfunction and diastolic heart failure. *Heart*. 2006; 92(5):712-718.
45. Li Y., Li Z., Zhang C., Li P., Wu Y., Wang C., Bond Lau W., Ma X. L., Du J. Cardiac fibroblast-specific activating transcription factor 3 protects against heart failure by suppressing MAP2K3-p38 signaling. *Circulation* 2017; 135:2041–2057
46. Liu T, Song D, Dong J, Zhu P, Liu J, Liu W, Ma X, Zhao L, Ling S. Current Understanding of the Pathophysiology of Myocardial Fibrosis and Its Quantitative Assessment in Heart Failure. *Front Physiol* 2017; 8:238.
47. Liu W, Wang Z. Current understanding of biomechanics of ventricular tissues in heart failure. *Bioengineering* 2019; 7(2): doi:10.3390.
48. Liu Y, Afzal J, Vakrou S, Greenland GV, Talbot CC, Hebl VB, Guan Y, Karmali R, Tardiff JC, Leinwand LA, Olgin JE, Das S, Fukunaga R, Abraham MR. Differences in microRNA-29 and pro-fibrotic gene expression in mouse and human hypertrophic cardiomyopathy. *Front Cardio Med* 2019; 6:170

49. Lobo L, Carvalheira J, Canada N, Bussadori C, Gomes JL, Faustino AMR. Histologic characterization of dilated cardiomyopathy in Estrela mountain dogs. *Vet Pathol* 2010; 47(4):637-642.
50. Lopez B, Gonzalez A, Ravassa S, Beaumont J, Moreno M, San Jose G, Querejeta R, Diez J. Circulating biomarkers of myocardial fibrosis: the need for a reappraisal. *J Am C Cardio* 2015;65(22):2449-2456
51. Marber, M.S.; Rose, B.; Wang, Y. The p38 mitogen-activated protein kinase pathway-A potential target for intervention in infarction, hypertrophy, and heart failure. *J. Mol. Cell. Cardiol.* 2011, *51*, 485–490.
52. McNally EM, Golbus JR, Puckelwartz MJ. Genetic mutations and mechanisms in dilated cardiomyopathy. *J of Clin Inves* 2013; 123(1):19-26
53. McNally EM, Mestroni L. Dilated cardiomyopathy: genetic determinants and mechanism. *Circ Res* 2017; 121(7):731-748.
54. McKenna WJ, Judge DP. Epidemiology of the inherited cardiomyopathies. *Nat Review* 2020; 18:22-36.
55. Meng Q, Bhandary B, Bhuiyan MS, James J, Osinska H, Valiente-Alandi I, Shay-Winkler K, Gulick J, Molkentin JD, Blaxall BC, Robbins J. Myofibroblast-specific TGFbeta receptor II singaling in the fibrotic response to cardiac myosin bidning protein C induced cardiomyopathy. *Mol Med* 2018; 123:1285-1297.
56. Molkentin JD, Bugg D, Ghearing N, Dorn LE, Kim P, Sargent MA, Gunaje J, Otsu K, Davis JM. Fibroblast-specific genetic manipulation of p38 mitogen-activated protein kinase *in vivo* reveals its central regulatory role in fibrosis. *Circulation* 2017; 136:549–561
57. Munch J, Abdelilah-Seyfried S. Sensing and responding of cardiomyocytes to changes of tissue stiffness in the diseased heart. *Front Cell Dev Bio* 2021; 9:642840.
58. Perestrelo AR, Silva AC, De La Cruz JO, Martino F, Horvath V, Caluori G, Polansky O, Vinarsky V, Azzato G, de Marco G, Zampachova V, Skladal P, Pagliari S, Rainer A, Pinto-do-O P, Carvella A, Koci K, Nascimento DS, Forte G. Multiscale analysis of extracellular matrix remodeling in the failing heart. *Circ Res* 2020; 128:24-38.
59. Powers JD, Kooiker KB, Mason AB, Teitgen AE, Flint GV, Tardiff JC, Schwartz SD, McCulloch AD, Regnier M, Davis J, Moussavi-Harami F. Modulating the tension-time integral of the cardiac twitch prevents dilated cardiomyopathy in murine hearts. *JCI Insight* 2020; 5(20):e142446
60. Raman B, Ariga R, Spartera M, Sivalokanathan S, Chan K, Dass S, Petersen SE, Daniels MJ, Francis J, Smillie R, Lewandowski AJ, Ohuma, EO, Rodgers C, Kramer CM, Mahmod M, Watkins H, Neubauer S. Progression of myocardial fibrosis in hypertrophic cardiomyopathy: mechanisms and clinical implications, *European Heart Journal - Cardiovascular Imaging* 2019; 20(2):157–167
61. Reichardt IM, Robeson KZ, Regnier M, Davis J. Controlling cardiac fibrosis through fibroblast state space modulation. *Cell Sig* 2021; 79: 109888.
62. Reinoso TR, Landim-Vieira M, Shi Y, Johnston JR, Chase PB, Parvatiyar MS, Landstrom AP, Pinto JR, Tadros HJ. A comprehensive guide to genetic variants and post-translational modification of cardiac troponin C. *J Musc R Cell Mot* 2020
63. Rupert CE, Kim TY, Choi B, Coulombe KLK. Human cardiac fibroblast number and activation state modulate electromechanical function of hiPSC-cardiomyocyte in engineered myocardium. *Stem Cell Int.* 2020; 9363809

64. Schultheiss HP, Fairweather D, Caforio ALP, et al. Dilated cardiomyopathy. *Nat Rev Dis Primers*. 2019;5(1):32.
65. Sewanan LR, Schwan J, Kluger J, Park J, Jacoby DL, Qyang Y, Campbell SG. Extracellular matrix from hypertrophic myocardium provokes impaired twitch dynamics in healthy cardiomyocytes. *JACC B Trans Sci* 2019; 4(4):495-505.
66. Turner NA, Blythe NM. Cardiac fibroblast p38 MAPK: a critical regulator of myocardial remodeling. *J Cardiovas Dev Dis* 2019; 6:27.
67. Tuttle AH, Philip VM, Chesler EJ. Mogil JS. Comparing phenotypic variation between inbred and outbred mice. *Nat Methods* 2018; 15**:**994–996.
68. Wang D, Robertson IM, Li MX, McCully ME, Crane ML, Luo Z, Tu A, Daggett V, Sykes BD, Regnier M. Structural and functional consequences of the cardiac troponin C L48Q Ca2+-sensitizing mutation. *Biochem* 2012; 51:4473-4487
69. Wang D, McCully ME, Luo Z, McMichael J, Tu A, Daggett V, Regnier M. Structural and functional consequences of cardiac troponin C L57Q and I61Q Ca2+ desensitizing variants. *Arch Biochem Biophys* 2013; 535(1)
70. Ward M, Iskratsch T. Mix and (mis-)match – the mechanosensing machinery in the changing environment of the developing, healthy adult and diseased heart. *BBA Mol Cell R* 2020; 1867:118436.
71. Zhong ZA, Sun W, Chen H, Zhang H, Lay YE, Lane NE, Yao W. Optimizing tamoxifen-inducible Cre/loxp system to reduce tamoxifen effect on bone turnover in long bones of young mice. *Bone.* 2015 Dec;81:614-619.